

Review

Recent Advances in Transition Metal Carbide Electrocatalysts for Oxygen Evolution Reaction

Yuanfei Wang [†], Qimeng Wu [†], Bicheng Zhang [†], Lei Tian [†], Kexun Li ^{*} and Xueli Zhang ^{*}

College of Environmental Science and Engineering, Nankai University, 94 Weijin Road, Tianjin 300071, China; 1710659@mail.nankai.edu.cn (Y.W.); 1710665@mail.nankai.edu.cn (Q.W.); 1710679@mail.nankai.edu.cn (B.Z.); 1710657@mail.nankai.edu.cn (L.T.)

^{*} Correspondence: likx@nankai.edu.cn (K.L.); 1120190190@mail.nankai.edu.cn (X.Z.);

Tel.: +86-156-2043-2665 (K.L.); +86-150-8310-4134 (X.Z.)

[†] The four first authors share same contribution to this article.

Received: 15 September 2020; Accepted: 5 October 2020; Published: 11 October 2020



Abstract: The electrolysis of water is considered to be a primary method for the mass production of hydrogen on a large scale, as a substitute for unsustainable fossil fuels in the future. However, it is highly restricted by the sluggish kinetics of the four-electron process of the oxygen evolution reaction (OER). Therefore, there is quite an urgent need to develop efficient, abundant, and economical electrocatalysts. Transition metal carbides (TMCs) have recently been recognized as promising electrocatalysts for OER due to their excellent activity, conductivity, and stability. In this review, widely-accepted evaluation parameters and measurement criteria for different electrocatalysts are discussed. Moreover, five sorts of TMC electrocatalysts—including NiC, tungsten carbide (WC), Fe₃C, MoC, and MXene—as well as their hybrids, are researched in terms of their morphology and compounds. Additionally, the synthetic methods are summarized. Based on the existing materials, strategies for improving the catalytic ability and new designs of electrocatalysts are put forward. Finally, the future development of TMC materials is discussed both experimentally and theoretically, and feasible modification approaches and prospects of a reliable mechanism are referred to, which would be instructive for designing other effective noble-free electrocatalysts for OER.

Keywords: oxygen evolution reaction; transition metal carbides; mechanism; hybridization; morphology modification

1. Introduction

With the development of science and technology, the contradiction between the increasing demand for resources and the limitations of traditional energy has become increasingly prominent. Hydrogen energy has the characteristics of a high energy density and safe by-products, so it is an ideal substitute for carbon-based fuel [1–5]. In recent years, researchers have been trying to find technologies for large-scale hydrogen production, but almost all of these methods, including the alkaline water splitting reaction, metal–air battery, and fuel cell, inevitably rely on a dual electrode system. Generally speaking, this kind of system consists of two parts: The oxygen reduction reaction (ORR: $O_2 + 4e^- + 4H^+ \rightarrow 2H_2O$ or $O_2 + 4e^- + 2H_2O \rightarrow 4OH^-$) or hydrogen evolution reaction (HER: $4H^+ + 4e^- \rightarrow 2H_2$ or $4H_2O + 4e^- \rightarrow 2H_2 + 4OH^-$) that occurs in the cathode part, and the oxygen evolution reaction (OER: $2H_2O \rightarrow 4H^+ + 4e^- + O_2$ or $4OH^- \rightarrow 2H_2O + 4e^- + O_2$) that takes place in the anode part.

Restricted by the slow four-electron transfer process [6–8], OER is more likely to block the total reaction than HER, which is merely a two-electron reaction [9]. The sluggish kinetic process of OER requires a higher potential to cross the energy barrier, thus greatly increasing the cost of the reaction. As a matter of fact, electrocatalysis is considered to be the most effective way to accelerate the kinetic

process and reduce the cost [10,11]. However, the original electrocatalysts were noble metals, such as platinum and ruthenium, especially their oxides, which had a satisfactory catalytic effect, but could not be widely used due to their high cost [12–14].

Currently, transition metal carbides (TMCs), which have served as typical representatives of burgeoning non-metal electrocatalysts, have attracted much attention due to their high electrical conductivity, satisfactory mechanical strength and hardness, and excellent stability. After much effort over a long period of time [15], researchers have gradually realized that TMCs and their rich hybrid materials exhibit excellent OER performances. For example, Tang et al. [16] successfully synthesized an Mo/Co carbide electrocatalyst, which was applied to OER and displayed a low overpotential and good stability, showing advantages of hybrid electrocatalysts over traditional ones. Very recently, the emerging nanotechnology improves the practical application of TMCs in OER because it helps to overcome the large energy loss caused by the high-temperature calcination synthesis method and is extremely beneficial for the constructing of surface morphology [17]. Therefore, TMC electrocatalysts with a composite morphology perform a good application prospect in the OER field. Benchakar et al. reported a TMC electrocatalyst fabricated by coupling cobalt layered double hydroxide (Co-LDH) on $Ti_3C_2T_x$ MXene, and it exhibited promising catalytic activity for OER [18]. Munir et al. [19] synthesized Ni/Ni₃C nanoparticles (NPs) encapsulated in N-enriched carbon nanotubes (CNTs) and they demonstrated that the exceptional activity for OER were attributed to the synergistic effect between Ni/Ni₃C and CNTs. All the above examples support that hybridization and composite morphology play quite an essential role for OER in recent studies [20,21]. Therefore, the rapid development of TMC electrocatalytic materials urgently needs to be comprehensively reviewed in light of recent progress. Wang et al. [22] briefly summarized the synthesis and application of TMCs. At the same time, they paid full attention to the hybridization of TMC materials, which was proved to be one of the decisive factors affecting the catalytic performance. Unfortunately, the research on TMC electrocatalysts is still very limited.

In this paper, TMCs are classified into five sections—NiC, WC, Fe₃C, MoC, and MXene—according to their intrinsic properties and main structures. The mechanism analysis, designed synthesis methods, and OER performance of TMCs are discussed in detail. Several new developments of OER are also analyzed from both theoretical and experimental aspects. In the second section, the basic parameters and measurement standards for evaluating electrocatalysts are introduced. In the third part, application examples of the above five types of electrocatalysts and their hybrids in the OER field are described at length. It is worth mentioning that MXene material has been relatively less studied, but it shows a good application prospect of OER, so this paper mainly introduces it. Finally, we make a brief summary of the whole research field, and put forward new views on the material synthesis, morphology and structure, hybrid method, theoretical development, and mechanism in different conditions of OER electrocatalysts, in order to benefit future research.

2. Parameters and Mechanism for OER

Generally speaking, OER electrocatalysts are catalytic materials, which can be coated on the electrode surface or as the electrode itself. With high conductivity and special structure, the catalysts accelerate the sluggish four-charge transfer process by absorbing reactants on the electrode surface, which helps to overcome kinetic obstacles and reduce energy loss. Therefore, in order to objectively analyze the performance of electrocatalysts, we need to introduce a series of specific evaluation systems and parameters. To better explain the whole OER process and TMC catalysts, Section 2.1 briefly introduces the key parameters and Section 2.2 clarifies the measurement standards. Importantly, the following parameters constitute a comprehensive evaluation system of an electrocatalyst based on the standard evaluation conditions established by McCrory et al. [23].

2.1. Parameters and Measurement Criteria for OER

2.1.1. Overpotential (η)

Overpotential (η) is a basic parameter to evaluate the performance of electrocatalysts. Theoretically, according to Gibbs free energy formula (Equation (1)), the potential of OER can be acquired and it is 1.23 V vs. reversible hydrogen electrode (RHE). In this equation, ΔG denotes Gibbs free energy change, n implies the number of transferred electrons, and F and E_{eq} are the Faraday constant and standard electromotive force, respectively. It is essential to note that this thermodynamic potential (1.23 V) for OER is defined in the case of standard condition (25 °C and 1 atm) and equilibrium state. However, since the OER, which is a four electron-proton coupled reaction, requires more energy to overcome the kinetic barrier caused by electron transfer process, the reaction needs a working potential that is higher than the equilibrium value. Overpotential (η) is defined as the difference between the two potentials in Equation (2), in which E is the applied potential. If $\eta = 0$, $E = E_{eq}$, the reaction is at equilibrium condition and total net current is zero [24].

$$\Delta G = -nFE_{eq} \quad (1)$$

$$\eta = E - E_{eq} \quad (2)$$

Therefore, the overpotential (η) can be understood as the excess energy required to achieve a specific current density and the electrocatalysts with a lower overpotential are more suitable for OER. Additionally, the two most commonly used potential values as electrocatalyst evaluation criteria are the onset overpotential of OER (η_0) and the overpotential when the current density is equal to 10 mA/cm² (η_{10}). Among them, the onset overpotential is the point that indicates a sudden increase of current density, while η_{10} implies that the commercially equivalent photoelectrochemical water splitting efficiency equals 12.3%. Therefore, it is appropriate to choose these two values as a widely accepted standard [25]. The main approach to calculating the overpotential of an electrocatalyst is to normalize the polarization curves of cyclic voltammetry (CV) and linear sweep voltammetry (LSV) to obtain the potential values under different exchange current densities, and the overpotential can be acquired by then subtracting the equilibrium potential.

2.1.2. Tafel Slope

In the assessment methods of the properties of electrocatalysts, the Tafel slope (b) plays an essential role. To better interpret the Tafel slope, the exchange current density (i_0) will be discussed first. For a certain electrochemical reaction, the total current (j) is the sum of currents in both the anode (j_a) and cathode (j_c) (Equation (3)); more importantly, according to the famous Butler–Volmer (B-V) equation (Equation (4)), α_a and α_c refer to the transfer coefficient in the anode and cathode, respectively. n denotes the number of electrons transferred in the reaction and F indicates the Faraday constant, whilst R and T represent the universal gas constant and absolute temperature, respectively. Moreover, j_0 is the exchange current, which can be divided by the electrode area (A), so the exchange current density (i_0) is obtained in Equation (5).

$$j = j_a + j_c \quad (3)$$

$$j = j_0[\exp(\alpha_a n F \eta / RT) - \exp(\alpha_c n F \eta / RT)] \quad (4)$$

$$j_0 / A = i_0 \quad (5)$$

The B-V Equation (Equation (4)) can be simplified to the form of Equation (6), which is originally put forward by Tafel as an empirical formula, in which a refers to the overpotential at a current density of 1 mA/cm² and b is the Tafel slope.

$$\eta = a + b \log(j) \quad (6)$$

Considering that the Tafel slope (b) represents “the potential rise corresponding to the increase of unit exchange current density”, it is obvious that a lower Tafel slope (b) indicates a higher current increasing efficiency, which refers to a more promising electrocatalyst. Tafel slope (b) is also an indicator clarifying the rate determining step (RDS) of the whole process of water splitting reaction, including Volmer mechanism, Volmer–Tafel mechanism, and Volmer–Heyrovsky mechanism [26]. The profound role of Tafel slope (b) in OER mechanism needs to be further studied.

2.1.3. Electrochemically Active Surface Area (ECSA)

It has to be pointed out that the electrochemically active surface area (ECSA), which can be measured by means of testing double-layer capacitance (C_{dl}), is an indispensable measurement parameter for a given electrocatalyst, especially for porous substrate materials. Through analysis of CV polarization curve, there is enough evidence to prove that in the non-Faradaic overpotential region (0.1 V window area near the open-circuit voltage region), all the current changes are because of the charge-discharge processes of double-layer capacitance (C_{dl}). The charging current (i_c) varies at different scan rates (v), so Equation (7) is frequently utilized to calculate the value of C_{dl} ; as the slope of i_c - v curve equals to C_{dl} , the method is precise and practical. When C_{dl} is known, the magnitude of ECSA can be easily obtained with Equation (8). C_s is the specific capacitance of each sample, and for transition metals, C_s often ranges from 20 to 60 $\mu\text{F}\cdot\text{cm}^{-2}$ [27].

$$i_c = vC_{dl} \quad (7)$$

$$\text{ECSA} = C_{dl}/C_s \quad (8)$$

A relatively high ECSA, which certifies that there are sufficient coordination unsaturated atoms and exposing active sites in the catalyst, implicates a better catalytic performance.

2.1.4. Faradaic Efficiency (FE)

Faradaic efficiency (FE), which can be calculated by the ratio between the effective oxygen yield and the theoretical oxygen evolution, is a special parameter employed to evaluate the performance of electrocatalysts and implies the efficiency of electrons involved in an electrochemical reaction. However, FE is often not accounted for by researchers, who just assume it as 100%; as a result, the effect of some catalysts is overestimated, leading to the consequence that a proportion of the research is invalid. In fact, the FE plays an essential role in the assessment procedure as it indicates the ultimate effect of OER. In different cases, the catalytic performance of electrocatalysts may differ somewhat, especially when phase change and substance decomposition exist.

2.1.5. Electrochemical Impedance Spectroscopy (EIS)

Electrochemical impedance spectroscopy (EIS) is a safety disturbance technique that is often used to detect the internal process of an electrochemical system and measure the impedance of a battery in a certain frequency range. These data can determine the state of health (SOH) and state of charge (SOC) of the battery. In the case of its use for OER, it is also one important module of the electrochemical workstation and essential for the conductivity test of electrocatalysts. EIS test is significant for OER kinetics research. By measuring the position and size of semicircle region in EIS, the voltage of solution resistance loss can be obtained, and normalization of LSV curve can then be completed. Apart from that, EIS test also helps to analyze the impedance changes with specific morphological transformation, representing an assisted approach in material evaluation.

2.1.6. Stability

Apart from the above parameters, long-term stability, which has a close connection to the practical use of electrocatalysts, undoubtedly plays an important role in OER evaluation process. Most often,

we test the stability of materials by accelerated CV detection or a long-time (>10 h) constant voltage (current) test, and there should be no obvious current falling occurring for acceptable electrocatalysts. For all kinds of electrocatalysts, stability is always a problem needs to be solved [28].

2.2. Mechanism for OER

As introduced in Section 2.1, the applied potential of OER is much higher than the theoretical one at equilibrium state, which is 1.23 V vs. RHE. The total overpotential consists of overpotential in anode (η_a) and cathode (η_c) and the Ohm polarization overpotential (η_o). Ohm polarization overpotential is caused by contact resistance of solution, and can be measured by EIS test mentioned in Section 2.1.5 and reduced by optimizing the design of electrolytic cells (Equation (9))

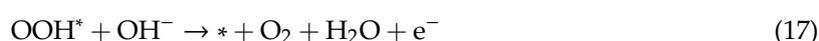
$$\eta = \eta_a + \eta_c + \eta_o \quad (9)$$

Therefore, η_a and η_c are the main factors which lead to a high applied potential, with the parameters above, we can assess the performance of electrocatalysts through the overpotential test. However, another problem then arises. For OER, the half reaction of water splitting reaction shows different reaction paths in acidic and alkaline conditions. As a result, in different measurement backgrounds, the experimental data, even for the same electrocatalysts, are totally diverse. In order to maintain the consistency of the experimental result of electrocatalysts fabricated in a wide variety of methods, McCrory et al. set a widely accepted standard for the testing environment considering various measurement techniques and conditions. They suggested that, for alkaline electrolytes, the medium is 1.0 M NaOH, while for acid electrolytes, 1.0 M H₂SO₄ is recommended. The main function of the media is to provide the reaction with the environment that electrons can transfer intermediates through [29].

The detailed mechanism of OER can be obtained through density functional theory (DFT). Yu et al. [30] studied the OER mechanism in acidic solution and proposed the four-step elementary reactions as follows, in which * denotes the active site on electrocatalysts.



It is significant to note that in this mechanism model, metal dissolution and corrosion are not considered due to the stability of metal carbides. The author also indicates that MC₂ (M refers to metal), with increased carbon content, behave better corrosion resistance towards acid solution. With the protection of carbon atoms, metals are prevented from being exposed to the surface, thus increasing the stability of electrocatalysts. Besides, the mechanism in neutral and alkaline media have been widely investigated as the equations below [31].



Note that in the above reactions, chemical groups such as O, OH, and OOH, are absorbed on the active sites (*) of catalysts, including physical or chemical absorption with no radicals involved as many literatures reported [31–36]. Generally, the formation of intermediates O* (Equation (15)) and OOH* (Equation (16)) has been considered as RDS for OER, and previous literature has reported

that TMCs are of great value to decrease overpotential for OER as it usefully accelerates RDS in kinetic process [32]. For instance, Ouyang et al. [33] found out that oxygen was favorable to Co sites adjacent to β - Mo_2C , because the doping of β - Mo_2C created a heterointerface and thus effectively lowered the energy barrier. In addition, the research of Wang et al. [34] suggests the similar conclusion. Their study revealed that Ni- Ni_3C exhibited smaller Gibbs free energy change (1.815 eV) for the RDS than Ni (3.877 eV) and Ni_3C (3.701 eV), indicating the important role of Ni_3C , which efficiently accelerating kinetic process, thus decreasing the overpotential. Note that in different conditions, carbon atoms play diverse roles but similarly contributing to enhancing OER performance [35]. In the mechanism research, DFT calculation is essential, but the drawback of which is also clear. Since particles like Co and Fe_3C may be oxidized at OER potential, the mechanism under harsh oxidative conditions is still not confirmed [36], including oxidation in the bulk or only on the surface of TMC electrocatalysts.

With the understanding of OER evaluation parameters and mechanism, we have lucid and unified criteria to assess the performance of electrocatalysts, which makes it possible to find promising catalysts for OER.

3. Transition Metal Carbide Electrocatalysts for OER

3.1. Synthesis Methods of TMCs

Firstly, the typical synthetic methods of TMCs need to be introduced. Syntheses of TMCs can be divided into template-free method and template-assisted method, both of which are based on a high-temperature carbothermal reaction. For example, in the template-free method, metals and carbon are usually heated directly above 800 °C. The difference is that in the template-assisted method, templates such as metal organic framework (MOF), are first made, after that, the synthesized templates are burned. The distinction between the two methods lies in the control of structure and composition, the template-free method has a poor control effect, while the template-assisted method has a better operability.

Through different synthesis methods, we can obtain various structures of electrocatalysts, such as nanodots, nanowires, two-dimensional (2D) layered structure, core-shell structure, and mosaic structure. A wide variety of examples will be discussed in detail based on experimental results as Table 1 displays.

Table 1. Important transition metal carbide catalysts employed for water splitting reaction.

Catalysts	Overpotential (mV) for OER at a Specific Current Density	Synthesis Strategies	Reference
MXene			
Co-P/3D Ti ₃ C ₂ MXene	298 @ 10 mA·cm ⁻²	Constructing aggregation-resistant 3D MXene architecture via a capillary-forced assembling strategy (template free).	[37]
Ni _{0.7} Fe _{0.3} PS ₃ @ Ti ₃ C ₂ T _x	282 @ 10 mA·cm ⁻²	Decorating nickel-based bimetal phosphorus trisulfide nanomosaic on the surface of MXene nanosheets (template free).	[38]
IrCo @ ac-Ti ₃ C ₂	220 @ 10 mA·cm ⁻²	Incorporating IrCo into basal-plane-porous titanium carbide MXene (template free).	[39]
TCCN	420 @ 10 mA·cm ⁻²	Free-standing flexible films with hierarchically porous structure was constructed from 2D graphitic carbon nitride and titanium carbide nanosheets (template free).	[40]
Ti ₃ C ₂ T _x -CoBDC	410 @ 10 mA·cm ⁻²	Hybridizing 2D cobalt 1,4-benzenedicarboxylate (CoBDC) with Ti ₃ C ₂ T _x nanosheets via an interdiffusion reaction-assisted process (template free).	[41]
CoNiPS ₃ /C	262 @ 30 mA·cm ⁻²	Simultaneous phosphorization and sulfurization processes and Co-Ni Prussian-blue analogues (PBA) as templating precursor (template assisted).	[42]
Fe₃C (Cementite)			
Fe ₃ C/Fe ₂ O ₃ @ NGNs	-	Assembling graphene oxide with graphitic carbon nitride and FeOOH nanorods, nanostructure of carbon layers coated iron species was constructed (template free).	[43]
Fe @ C-NG/NCNTs	450 @ 10 mA·cm ⁻²	Annealing a Fe-based MOF (MIL-88B) loaded with melamine at 800 °C in N ₂ to get a hybrid structure (template assisted).	[44]
NiC			
Fe-Ni ₃ C-2%	275 @ 10 mA·cm ⁻²	Carburizing treatment is carried out in argon/H ₂ atmosphere and then dope heteroatom of Fe into Ni ₃ C nanodots via a co-precipitation method (template assisted).	[45]
NiC/MoC/NiMoO ₄	280 @ 10 mA·cm ⁻²	After preparing NiMoO ₄ /NF nanorod arrays, NiMoO ₄ nanorods react with dopamine at a high annealing temperature to form 3D NiC/MoC/NiMoO ₄ (template assisted).	[46]
Co-Ni ₃ C/Ni @ C	325 @ 10 mA·cm ⁻²	Co-Ni ₃ C/Ni @ C is prepared via pyrolysis of the bimetallic MOF (Co/Ni-BTC) (template assisted).	[47]
d-NiC _{0.2} NS/Ni/CF	228 @ 10 mA·cm ⁻²	Nanosheets are prepared on nickel-coated copper foil by mild electrodeposition with high index polyhedral dendritic hexagonal NiC _x (template free).	[48]
Ni/NGNRs	380 @ 10 mA·cm ⁻²	Mix MWCNTs together with MERCK via a solvothermal process and then collect the resultant mixture for the post treatment of further heating under argon atmosphere (template free).	[49]
Mo₂C			
β-Mo ₂ C	267 @ 5 mA·cm ⁻²	Reduction of MoO ₃ with decolorizing carbon (Mo ₂ C-DC) and multiwalled carbon nanotubes (Mo ₂ C-MW) at 950 °C resulted in phase pure Mo ₂ C (template free).	[50]
Mo ₂ C @ CS	320 @ 10 mA·cm ⁻²	Mo ₂ C @ CS is synthesized through a one-pot process with ammonium molybdate and glucose as the Mo and C source (template free).	[51]
Ni-Mo ₂ C @ NC	328 @ 10 mA·cm ⁻²	NiMoO ₄ ·xH ₂ O nanobelts serve as a single source for the synthesis of both Ni and Mo _x C nanoparticles, while melamine simultaneously serves as the precursor and dopant for the formation of Ni-Mo ₂ C @ NC (template assisted).	[52]
B ₃ N:Mo ₂ C @ BCN	360 @ 100 mA·cm ⁻²	Obtaining hybrid structure via an eco-friendly organometallic complex of Mo imidazole and boric acid (template assisted).	[53]

3.2. Nickel Carbide

Among common transition metal carbides, nickel carbide has the advantages of a high cost efficiency and great electric conductivity. Therefore, it is suitable for the manufacturing of high-performance electrocatalyst for OER. In 1988, Zhao et al. publicized the fabrication of highly disordered hexagonal NiC_x filaments by chemical vapor deposition (CVD) [54]. After that, hexagonal NiC_x with other forms of nickel carbide constituted the nickel carbide family, and moreover, provided us with valuable alternative materials as promising HER and OER electrocatalysts.

One of the necessary factors for a good catalyst is a large surface area. Unless the material made of nickel carbide can reach a small particle size, its electrocatalytic performance will be reduced. In a way, smaller particle size means larger surface area, leading to more active sites during the process of reaction. Fadil et al. [55] reported atomically ordered Ni₃C, synthesized in the form of NPs smaller than

10 nm. Yang et al. [48] reported a facile route for the controllable orientation-dependent crystal growth of high-index faceted dendritic hexagonal NiC_x nanosheets on Ni-coated copper foil, with an optimized carbon content of 16.7 at %, by a mild electrodeposition approach (Figure 1). The material obtained was fully exposed $\{\bar{1}20\}$ high-index facets, contributing to improving the mass/electron transport capability and fully exposed active sites during the OER process. Impressively, the as-prepared material (denoted d- $\text{NiC}_{0.2}\text{NS}/\text{Ni}/\text{CF}$) exhibited remarkable catalytic activity (with overpotential of 121 and 228 mV at $10 \text{ mA}\cdot\text{cm}^{-2}$ for the HER and OER, respectively), simultaneously giving a nearly 100% Faradaic yield and affording a superior catalytic stability (beyond 100 h) as a bifunctional electrocatalyst for both the HER and OER in basic media.

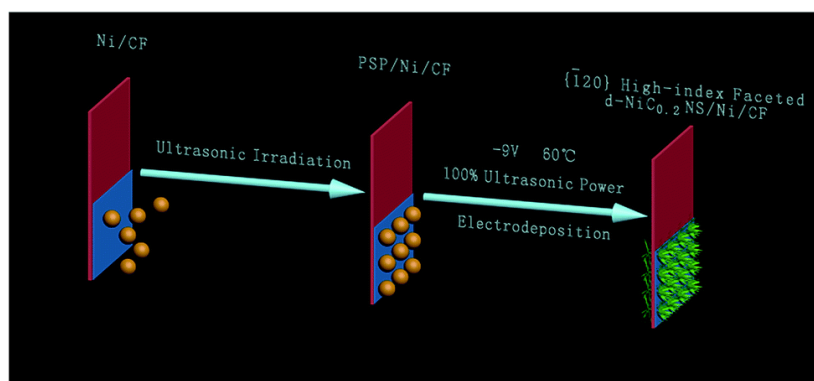


Figure 1. Schematic illustration of the synthetic route for d- $\text{NiC}_{0.2}\text{NS}/\text{Ni}/\text{CF}$. By using nickel sulfate and polystyrylpyridine resins (PSP) as the nickel and carbon precursor, the samples were obtained via a controllable and mild electrodeposition process with ultrasonic treatment at 60°C . Reproduced with permission from [48]. Copyright 2016 *Journal of Materials Chemistry A*.

Moreover, d- $\text{NiC}_{0.2}\text{NS}$ -coated copper foil (d- $\text{NiC}_{0.2}\text{NS}/\text{CF}$) samples, Pt/C-loaded CF and RuO_2/C -loaded CF (Pt/C/CF and $\text{RuO}_2/\text{C}/\text{CF}$) were prepared and then tested separately for a comparison. From the results, owing to its dendritic nanosheet morphology, optimized 16.7 at % carbon content, and fully exposed high-index facets, d- $\text{NiC}_{0.2}\text{NS}/\text{Ni}/\text{CF}$ displayed an improved mass/electron transport capability and fully exposed active sites, resulting in its high performance in OER and HER.

Although nickel carbide has a good catalytic effect on OER, it is actually more used to dope other elements or form a composite structure, such as Fe-doped [56], nitrogen-doped [57,58], and metal phosphide-mixed structure [47]. These electrochemical catalysts, most of which are doped with iron, nitrogen, or other metals, exhibit better results. For example, Haosen Fan et al. developed Fe-doped Ni_3C nanodots in N-doped carbon nanosheets [45]. In their experiment, by employing the method of carburization, 2D nickel-cyanide polymer precursors reacted and formed a structure in which Ni_3C nanodots were dispersed in ultra-thin N-doped carbon nanosheets. After the carburization process in Ar/H_2 atmosphere, 2D hybrid nanosheets with uniform Ni_3C nanodots embedded in N-doped carbon nanosheets were successfully obtained. The hybrid nanosheets had the lateral size of about 200–300 nm and thickness of about 10 nm, with uniform dispersion of 3–5 nm Ni_3C nanodots. When further doping heteroatoms of Fe in different amount into Ni_3C nanodots, the test results indicated that the 2 at % Fe-doped Ni_3C nanodot-based nanosheets (Fe- Ni_3C -2%) showed outstanding HER and OER properties, with a low overpotential (292 mV for HER and 275 mV for OER in 1.0 M KOH) and small Tafel slopes (34.6 mV dec^{-1} for HER and 62 mV dec^{-1} for OER in 1.0 M KOH). In addition, among these three catalysts, pure Ni_3C displayed less of an OER response, indicating that Fe doping can significantly improve the catalytic activity. The Fe- Ni_3C -2% catalyst also showed a small overpotential of 275 mV at an anode current density of $10 \text{ mA}\cdot\text{cm}^{-2}$, which is lower than those of pure Ni_3C and Fe- Ni_3C -5% samples.

In another example, Jaison Joy et al. reported the synthesis of nickel-incorporated nitrogen-doped graphene nanoribbon (Ni/NGNRs) through a facile solvothermal process [49]. After incorporating

nitrogen functionalities, graphene nanoribbon with tunable nickel content functions efficiently facilitated the water oxidation reaction and accelerated the catalytic reactivity, exhibiting an overpotential of 380 mV with a Tafel slope of 60 mV dec⁻¹ to sustain 10 mA·cm⁻² in 1.0 M KOH.

In addition, nickel carbide is often used to form a composite structure with other substances, such as transition metal [59], as well as their oxides and carbides [60], and some of them have intensive electrocatalytic properties for OER. For instance, Shuo Geng et al. synthesized a three-dimensional (3D) heterostructure NiC/MoC/NiMoO₄ electrocatalyst in a simple and feasible way [46]. As shown in Figure 2, NiMoO₄/NF nanorod arrays were synthesized by hydrothermal method with the precursors of NiMoO₄ nanorods and nickel foam (NF), which was the Ni source. Then, at a high annealing temperature, the reaction between NiMoO₄ nanorods and dopamine accounted for the conversion of NiMoO₄ to NiC/MoC, which led to the formation of NiC/MoC/NiMoO₄ heterostructure nanorod arrays.

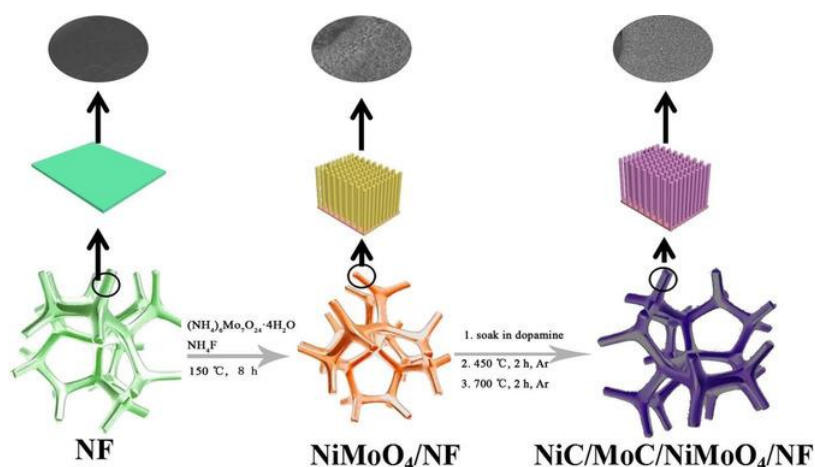


Figure 2. Schematic illustration of the synthesis process for NiC/MoC/NiMoO₄/NF. Reproduced with permission from [46]. Copyright 2019 *Chemistry-An Asian Journal*.

Through electrode performance test, the optimized NiC/MoC/NiMoO₄ behaved a low overpotential of 280 mV at a current density of 10 mA·cm⁻² in 1.0 M KOH for OER. Moreover, it showed quite low cell voltage of 1.52 V at 10 mA·cm⁻² and remarkable stability for more than 20 h, demonstrating the superiority of the NiC/MoC/NiMoO₄ heterostructure for OER. Besides, Qing Qin et al. [59] in situ synthesized Ni/Ni₃C core/shell hierarchical nanospheres through an ionic liquid-assisted hydrothermal method at a relatively low temperature. Resulting from the high electrical conductivity, more exposed active sites, and core–shell interface effect, the material obtained exhibited superior OER performance with a low overpotential, small Tafel slope, and fantastic stability (with overpotential of 350 mV at 10 mA·cm⁻¹ and Tafel slopes of 57.6 mV dec⁻¹).

MOF is a crystalline material with a one or multi-dimensional network structure formed by coordination between metal ions and an organic complex. Due to the high surface area of MOFs, they serve as both homogeneous and heterogeneous catalytic sites. Furthermore, MOFs possess controlled pore structure. These peculiarities lead to the result that MOFs are widely applied in many fields, varying from industrial gas separation and storage [61] to heterogeneous catalysis [62] and sensing devices [63], including synthesis of high-performance electrocatalysts for OER. Jia et al. [64] prepared Co-doped Ni₃C/Ni embedded in a carbon matrix (Co-Ni₃C/Ni@C) by pyrolysis of bimetal-MOF (Co/Ni-MOF) under a flow of Ar/H₂ at 350 °C. The synthesis of the precursor bimetal-MOFs is displayed in Figure 3. Uniform cubic Co/Ni-BTC was constructed through a simple method. After carbonization at 350 °C under a flow of Ar/H₂ gas, Co-Ni₃C/Ni@C was obtained.

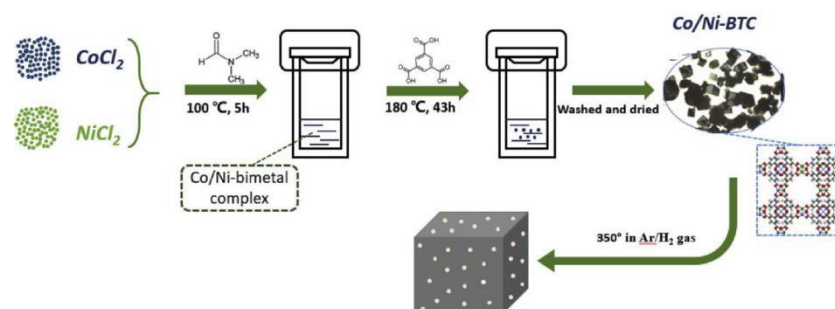


Figure 3. Schematic illustration of the synthetic route for Co/Ni-350. Reproduced with permission from [64]. Copyright 2019 *International Journal of Hydrogen Energy*.

For comparison, $\text{Ni}_3\text{C}/\text{Ni}@\text{C}$ was also prepared and then tested. As shown in Figure 4a, due to surface oxidation of the catalysts during OER, the oxidation peaks in the LSV curves appeared at ~ 1.35 V vs. RHE, meaning that Co- $\text{Ni}_3\text{C}/\text{Ni}@\text{C}$ showed a smaller onset overpotential (as introduced in Section 2.1.1, the onset overpotential can be obtained by means of using the potential where there is a sudden increase of exchange current density in the LSV curve to subtract 1.23 V) of 220 mV in comparison to $\text{Ni}_3\text{C}/\text{Ni}@\text{C}$ (290 mV) in the OER. Co- $\text{Ni}_3\text{C}/\text{Ni}@\text{C}$ also showed higher activity in the OER, reaching an overpotential of 325 mV at the current density of $10 \text{ mA}/\text{cm}^2$ (η_{10} can be obtained by means of using the potential at the current density of $10 \text{ mA}\cdot\text{cm}^{-2}$ to subtract 1.23 V), which is close to IrO_2 (330 mV) and lower than $\text{Ni}_3\text{C}/\text{Ni}@\text{C}$ (350 mV) (Figure 4b), indicating that Co-doping can significantly improve the catalytic activity. Besides, the Tafel plot (According to Equation (6), Tafel plot is the slope of $\log i$ -V curve, and a lower Tafel slope indicates better performance for OER) for Co- $\text{Ni}_3\text{C}/\text{Ni}@\text{C}$ (67.76 mV/dec) was much lower than $\text{Ni}_3\text{C}/\text{Ni}@\text{C}$ (112.45 mV/dec) and IrO_2 (79.92 mV/dec), verifying the efficient reaction kinetics in the OER (Figure 4c). As can be seen in Figure 4d, the LSV curves showed small negative variation after 1000 cycles, indicating its high stability in OER.

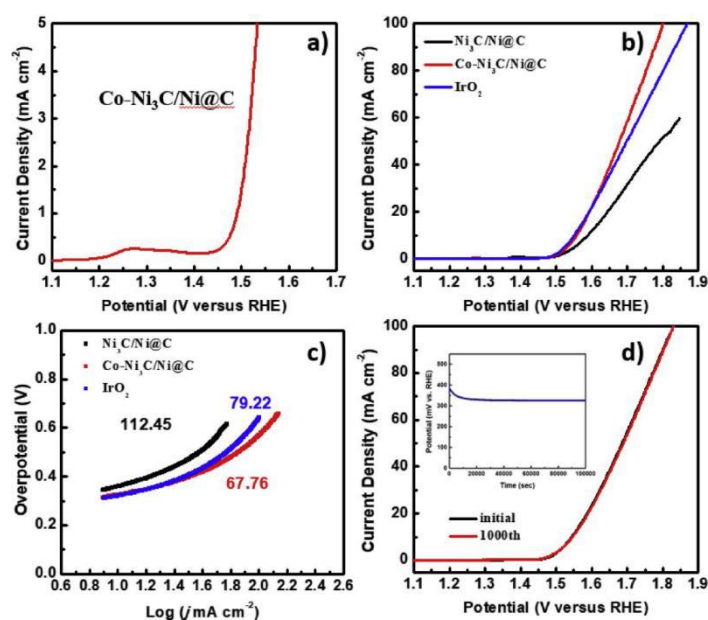


Figure 4. (a) OER polarization curves tested in 1.0 M KOH of Co- $\text{Ni}_3\text{C}/\text{Ni}@\text{C}$. (b) OER polarization curves tested in 1.0 M KOH of Co- $\text{Ni}_3\text{C}/\text{Ni}@\text{C}$, $\text{Ni}_3\text{C}/\text{Ni}@\text{C}$ and IrO_2 . (c) Tafel plots of different samples. (d) Polarization curves of Co- $\text{Ni}_3\text{C}/\text{Ni}@\text{C}$ before and after 1000 cycles, and the chronoamperometric response at a constant current of $10 \text{ mA}/\text{cm}^2$ of Co- $\text{Ni}_3\text{C}/\text{Ni}@\text{C}$. Reproduced with permission from [64]. Copyright 2019 *International Journal of Hydrogen Energy*.

3.3. Tungsten Carbide

Tungsten carbide (WC) was discovered to possess similar catalytic properties to those of platinum group metals for certain reactions by Levy and Boudart [65]. Therefore, it was considered as an attractive non-noble metal catalyst for proton exchange membrane (PEM) fuel cell applications. In general, there are two ways to synthesize tungsten carbide [66]. One of them is to first reduce a tungsten precursor to a reaction intermediate (usually tungsten powder). Then, the powder is carbonized at a high temperature in reductant atmosphere. The other way is to first obtain a highly active tungsten precursor (such as WO_3). The precursor powder is usually carbonized in H_2 and CH_4 mixed atmosphere. The electrocatalytic performance of product WC is affected by many factors, such as source materials, activation process, and preparation method. Therefore, exploring new carbonizing approaches is a method worth considering for improving the performance.

Although the performance of WC is inferior in direct comparison to platinum, WC has received much attention due to its low price and insensitivity to catalyst poisons, such as H_2S and CO [67,68]. Therefore, tungsten carbide became one of the most promising alternatives to noble metal electrocatalysts for the HER. Nevertheless, nothing has been reported on its application in the OER until the work of Han et al. [69] in 2018. In the experiment, they synthesized a superaerophobic nitrogen-doped tungsten carbide nanoarray electrode, exhibiting high stability and activity toward OER and effectively accelerating oxygen evolution in acid. In testing process, the performance of N-WC nanoarray toward OER was measured in 0.5 M H_2SO_4 , and for a comparison, commercial 20 wt % Ir/C and IrO_2 catalysts were measured. As displayed in Figure 5a, OER starts at about 1.35 V on the nanoarray electrode, while at about 1.5 V on commercial 20 wt % Ir/C and IrO_2 . The synchronized variation between voltage and O_2 concentration in Figure 5b demonstrated that OER really occurs at about 1.35 V vs. RHE. In addition, the current density increases drastically with potential, reaching up to $60 \text{ mA}\cdot\text{cm}^{-2}$ at about only 1.7 V vs. RHE.

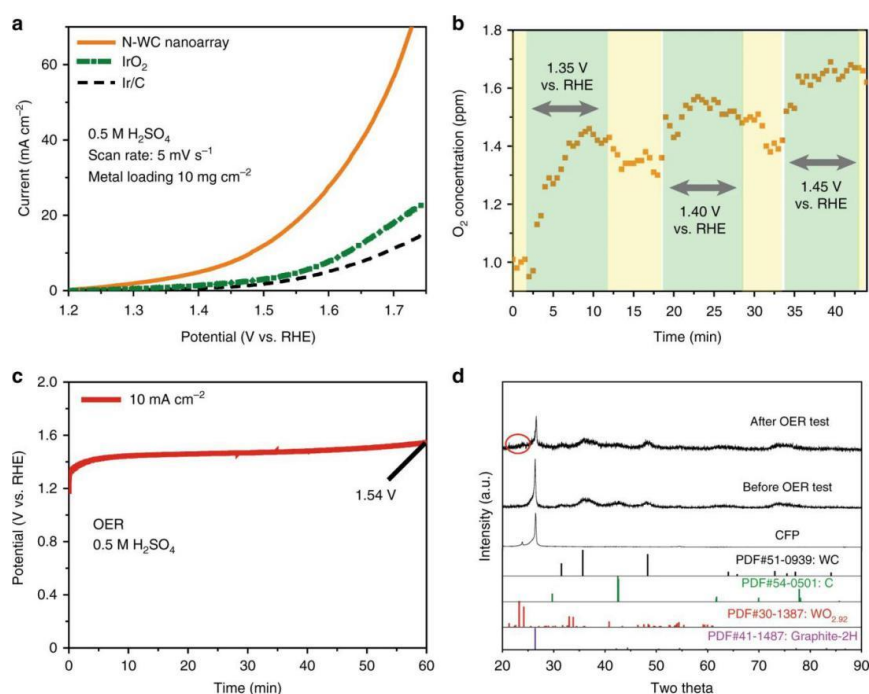


Figure 5. (a) OER polarization curves tested in 0.5 M H_2SO_4 of an N-WC nanoarray, IrO_2 , and 20 wt % Ir/C. (b) O_2 concentration in 0.5 M H_2SO_4 when different potentials are intermittently applied to an N-WC nanoarray electrode. (c) Stability test of an N-WC nanoarray for OER at $10 \text{ mA}\cdot\text{cm}^{-2}$. (d) X-ray diffraction (XRD) patterns of an N-WC nanoarray before and after an OER test. Reproduced with permission from [69]. Copyright 2018 *Nature Communications*.

Except for its instability, N-WC nanoarray is a promising electrocatalyst for OER. The XRD patterns of the nanoarray before and after the OER (Figure 5d) indicate that a small amount of tungsten oxides structured on the nanoarray, resulting in an increase of potential after 1 h of water splitting at $10 \text{ mA}\cdot\text{cm}^{-2}$ (Figure 5c). Although its catalytic stability is not satisfactory, N-WC nanoarray provides a research direction for noble-metal-free electrocatalysts in OER.

Regarded as a promising candidate for applications as a non-noble metal electrocatalyst for HER, WC itself is not a suitable catalyst for OER due to its high overpotential, which consequently leads to low electrocatalytic activity. In recent years, most researchers have preferred to study WC as an electrocatalyst substrate combined or doped with other substances, such as cobalt [70] and nitrogen [71]. Most of them are widely used in HER and ORR, while their application in OER is seldom reported. From the experiment carried out by Han et al. [69], tungsten oxides formed on the electrode during the process, which hindered the OER. This may be a possible reason why WC exhibited low electrocatalytic activity toward OER.

With the use of MOFs (Co^{2+} and W^{6+} as metal ions, and DMF as a ligand), Tao Zhao et al. [72] produced a material composed of porous nitrogen-doped carbon materials encapsulating cobalt and tungsten carbide (Co/W-C@NCNSs), working as a bifunctional catalyst for overall water splitting. They synthesized nanoscale MOFs through a microwave method and the MOFs obtained were then annealed under N_2 atmosphere at the temperature of 600°C and 800°C . Finally, the samples were obtained. The results show that, among the two samples obtained, Co/W-C@NCNSs (800°C) has better electrocatalytic activities, with an overpotential of 323 mV at a current density of $10 \text{ mA}\cdot\text{cm}^{-2}$ in the OER. Although the overpotential is not low enough compared with some noble-metal-based electrocatalysts, it has great potential to become an efficient electrocatalyst toward OER.

3.4. Iron Carbide

Iron carbide is a kind of intermetallic compound formed by iron and carbon, owning high conductivity and good stability [73–77]. The chemical formula of iron carbide is Fe_3C and it is usually applied for metal–air batteries [78–81]. The crystal structure of this material is a complex orthorhombic system, with high hardness, zero plasticity, and great brittleness. At present, the most common methods to prepare Fe_3C are reduction carburization, thermal decomposition, laser and CVD. The as-obtained morphology of Fe_3C is mainly powder, filled with carbon nanotubes or coated with carbon nanospheres. Fe_3C has many excellent properties and has been widely studied. How to further improve its performance and expand its application range have gradually become the main points of research in recent years.

Due to the combination of nitrogen atoms in graphite structure, nitrogen-doped carbon materials can perform impressive ORR catalytic activity. In addition, Defilippi et al. [82] took advantage of the sol–gel technique and successfully synthesized HfN NPs (less than 15 nm in diameter), which exhibited a quite low overpotential of 358 mV at $10 \text{ mA}\cdot\text{cm}^{-2}$ and long term stability as an OER electrocatalyst. This recent study indicates that metal nitrides possess high conductivity, stability, and melting point, and these properties make them qualified to be active both for ORR and OER. It has been shown that the electrocatalytic ability can also be developed by combining transition metals and metal oxides with carbon nitride materials [83]. At present, graphite carbonitride ($\text{g-C}_3\text{N}_4$) with 2D layered structure has been widely developed for effective OER and ORR electrocatalysts [84]. However, the relatively low conductivity and surface area of $\text{g-C}_3\text{N}_4$ seriously limit its application in electrocatalysis [85]. Therefore, the simple method shown in Figure 14 can be used to prepare N_3 -doped graphene-encapsulated $\text{Fe}_3\text{C}/\text{Fe}_2\text{O}_3$ heterostructures (named $\text{Fe}_3\text{C}/\text{Fe}_2\text{O}_3@\text{NGNs}$) to make it a better catalyst [43].

The polarization curves can be utilized to study the electrocatalytic activity of synthetic samples for ORR and OER. As shown in Figure 15a, the reduction peak of the metal-free N-doped graphene catalyst was positively shifted after the Fe element had been incorporated, thus the as fabricated $\text{Fe}_3\text{C}/\text{Fe}_2\text{O}_3@\text{NGNs}$ displayed a halfwave potential of 0.86 V, which was the same as commercial Pt/C. Simultaneously, $\text{Fe}_3\text{C}/\text{Fe}_2\text{O}_3@\text{NGNs}$, with an Tafel slope of 73 mV/dec, also outperformed NGNs and

Pt/C, indicating the gratifying kinetic process for ORR (Figure 15b). As for OER, the electrocatalyst showed an overpotential of 1.69 V at 10 mA·cm⁻² and a Tafel slope of 163 mV dec⁻¹ (Figure 15c,d). As a matter of fact, the enhanced ORR and OER performance could be attributed to the combination of the Fe₃C/Fe₂O₃ heterostructure, which provided more inherent active sites, thereby making this structure a promising dual-functional electrocatalyst.

Among many developed materials, Fe-N-C is considered a promising candidate. Especially in recent years, a large number of researchers have reported studies in which NPs, such as iron and/or its carbides, oxides, and nitride, are encapsulated in various N-doped carbon nano structures, such as CNTs, carbon layers, and carbon nanofibers. As a result, these modified materials exhibited satisfactory properties in some fields. Given the fact that some materials with a high surface area and large pore volume have poor electrical conductivity, conductive carbon materials such as graphene and CNTs must be introduced into them, in order to enhance catalytic ability. For instance, Zhao et al. [44] utilized porous, conductive NCNT/NPC hybrids, which possessed high density of Fe-N active sites, to fabricate a new catalyst named Fe₃C@NCNT/NPC and it exhibited excellently in OER.

Wang et al. [86] reported a new type of electrocatalyst, the construction of which is based on a CNT framework, with NPs of Fe and carbon embedded in it (called Fe@C-NG/NCNTs). Therefore, it provides us with an idea that it is possible to construct an electrocatalyst as a 'framework active site' structure with a large number of Fe-N_x active sites. DE (the potential gap between OER and ORR) is usually measured to reflect bifunctional activity of ORR/OER and a lower DE indicates better performance [87–89]. As shown in Figure 6, according to the curve, the DE value of Fe@C-NG/NCNTs is estimated to be 0.84 V, which is better than Pt/C catalyst (1.05 V). Therefore, Fe@C-NG/NCNTs seems to be of great value for research on bifunctional catalysts for ORR and OER.

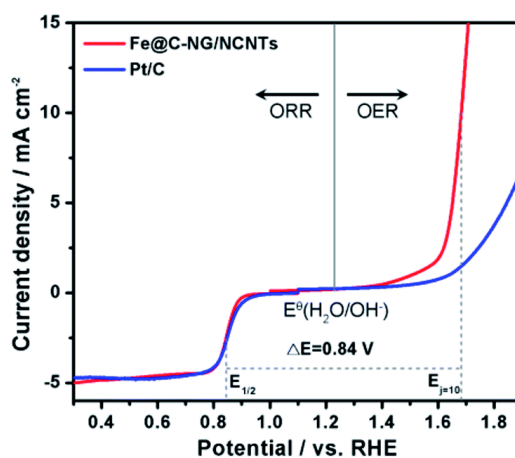


Figure 6. OER/ORR performance of Fe@C-NG/NCNTs and Pt/C is shown in the figure. Reproduced with permission from [86]. Copyright 2017 *Journal of Materials Chemistry A*.

Carbon materials functionalized with transition metal-based inorganic NPs can effectively improve electrocatalysis. For example, FeCo@NC core-shell nanospheres, with the carrier graphene, can be used as efficient dual-functional OER electrocatalysts [87]. Besides, Cui et al. [90] fabricated a great bimetal carbide-based bifunctional catalyst consisting of iron-molybdenum carbide (Fe₃Mo₃C) and IrMn nanoalloys, which was not only chemically stable in alkaline medium, but also in acidic environment. Under alkaline condition, the active OH* can be provided by free OH⁻ in the solution, while in acidic condition, the OH* just derived from the ionization of water. As a result, the alkaline medium is a more suitable environment for OER, thus the electrocatalysts can be more effective in alkaline condition.

3.5. Molybdenum Carbide

Molybdenum carbide (Mo_2C) has been extensively described as a low-cost catalyst for the HER [91–93], but, as for OER, it has not been reported until 2015 [50]. In a comparative experiment of transition metal carbides, Yagya N. Regmi et al. indicated that Mo_2C is the most active HER catalyst [94]. In addition, Fe_2N -type molybdenum carbide ($\beta\text{-Mo}_2\text{C}$) showed the best performance in HER activity and the lowest overpotential among materials synthesized via an amine-metal oxide composite intermediate. Morphology and surface structure of electrocatalysts often play an important role in their catalytic activities, and these physical characteristics vary with the synthesis methods. From this perspective, Yagya N. Regmi et al. [50] dived deeper into their research and indicated that Fe_2N -type Mo_2C displayed bifunctional catalytic activities. Therefore, it is believed to act as an OER electrocatalyst.

Although Mo_2C has shown great electrocatalytic performance in oxygen evolution activity, the stability still needs improving. An increasing number of researchers are studying how to convert it into nanomaterials, with an expectation of obtaining more efficient catalysts for OER. Due to excellent characteristics, graphite-like carbon nanomaterials (CNMs) have received great attention. Therefore, in the field of nanotechnology, the synthesis of CNMs is developing rapidly. Benefiting from high surface area, CNMs have been widely researched as a catalyst in electrochemical activities [95–97]. As a result, some researchers have been trying to apply CNMs in OER electrocatalysts, thus synthesizing molybdenum carbide coupled on carbon nanomaterials. For example, H. Wang et al. [51] designed highly crystalline Mo_2C NPs supported on carbon sheets ($\text{Mo}_2\text{C}/\text{CS}$) as a bifunctional catalyst toward HER and OER. The materials were obtained through a one-pot process where Mo was sourced from ammonium molybdate and carbon was from glucose (Figure 7).

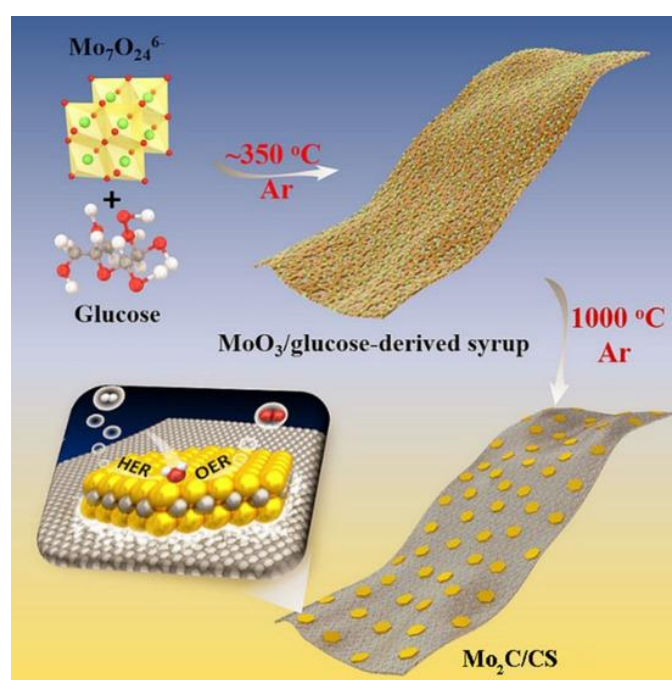


Figure 7. Schematic illustration of the synthetic process of an $\text{Mo}_2\text{C}/\text{CS}$ electrocatalyst for the oxygen evolution reaction. Reproduced with permission from [51]. Copyright 2017 *ChemSusChem*.

The result was that $\text{Mo}_2\text{C}/\text{CS}$ displayed excellent electrocatalytic performance, as well as a great stability over 100 h in the OER, with an overpotential of 320 mV at $10 \text{ mA}\cdot\text{cm}^{-2}$ in 1.0 M KOH.

According to theoretical calculations, nitrogen-doped carbon nanotubes (N-CNTs) show metallic behavior [98], meaning more active catalytic activity. Thus, a number of researchers were inspired to investigate methods on how to synthesize N-CNTs. Mo_2C combined with N-CNTs were designed

as effective electrocatalysts for the OER. Das D. et al. [52] developed a Ni/Mo_xC NPs-supported N-doped graphene/CNT hybrid catalyst, showing great bifunctionally catalytic activity toward both OER and HER. The overpotential was only 328 mV, while achieving a current density of 10 mA·cm⁻¹ in 1.0 M KOH. Apart from N-CNTs, nitrogen-doped carbon materials (N-CNMs), including carbon nanosheets, were applied for the OER. At the same time, materials based on molybdenum carbide combined with N-CNMs are usually doped with other transition metals, such as cobalt [99,100] and cobalt phosphide [101]. For instance, Zhu X. et al. [102] reported cobalt-doped β-molybdenum carbide encapsulated within nitrogen-doped carbon (Co_{0.1}-β-Mo₂C@NC), which showed superior catalytic activity toward OER. In the synthesizing process, bimetallic zeolitic imidazolate framework (ZIFs) of different Co/Zn mole ratios were saturated with a dimethylformamide (DMF) solution of MoO₂(acac)₂, and the mixture was calcined under nitrogen atmosphere at 900 °C (Figure 8). In the test for its electrocatalytic performance, the result of low overpotential of 262.2 mV at 10 mA·cm⁻¹ (in 1.0 M KOH) was outstanding. However, the large resistance which had a bad effect on water splitting limited its application.

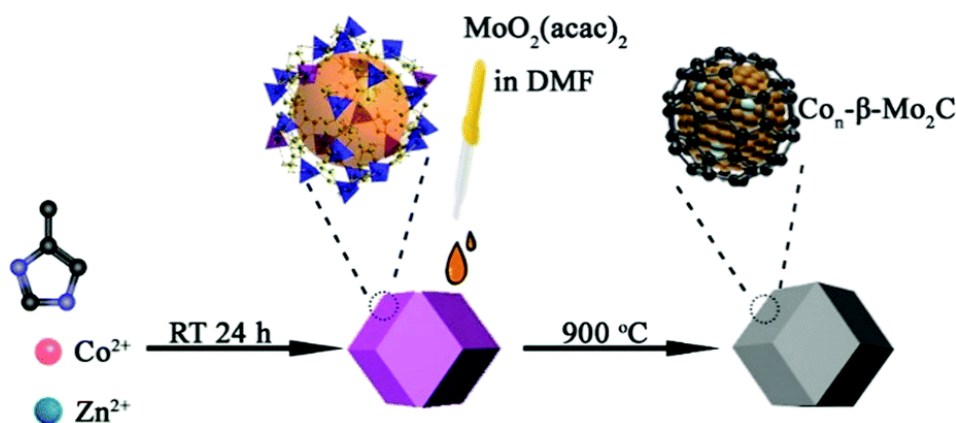


Figure 8. Schematic diagram of Co_n-β-Mo₂C@NC synthesis. Reproduced with permission from [102]. Copyright 2019 *Chemical Communications* (Cambridge England).

As mentioned earlier, cobalt-doped molybdenum carbide combined with N-CNMs has shown great catalytic activity in OER. Furthermore, it has been reported that materials based on Mo₂C-doped with two or more elements possess excellent catalytic activity. Anjum M.A.R. et al. [53] successfully synthesized boron and nitrogen co-doped molybdenum carbide NPs embedded in B,N-doped carbon networks (B,N:Mo₂C@BCN). With B and N doped, as well as formation of NPs embedded in BCN networks, the surface area was increased and charge transfer characteristics were improved, resulting in both great catalytic activity and a robust stability. For comparison, they also synthesized IrO₂, Mo₂C@C, and N:Mo₂C@C in the experiment. As displayed in Figure 9, the material obtained displayed excellent electrocatalytic performance and remarkable stability. It had a rather low overpotential, both before and after chronoamperometry (Figure 9a,b,e,f,h), and it still exhibited a relatively low Tafel slope of 61 mV dec⁻¹ (Figure 9c) and satisfactory stability after the durability test (Figure 9d,g).

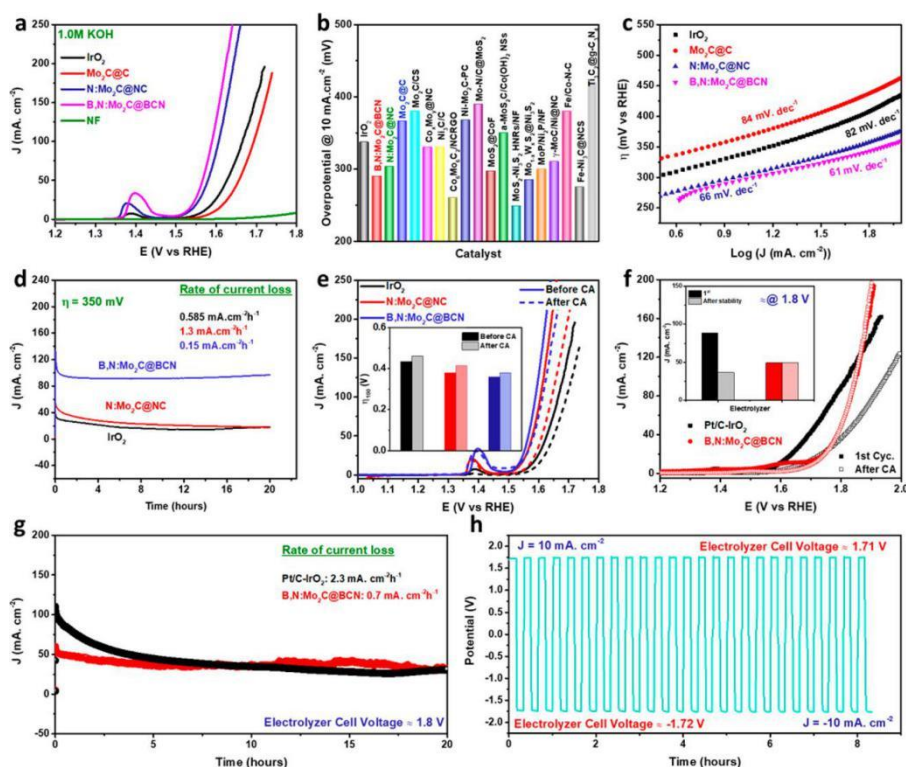


Figure 9. (a) OER IR-corrected polarization curves of Mo₂C@C, N:Mo₂C@NC, and B,N:Mo₂C@BCN catalysts in 1.0 M KOH loaded on an NF electrode. (b) Comparison of η_{10} values with other electrocatalysts based on Mo. (c) Tafel plots. (d) Electrode stability. (e) LSV curves and comparison of η_{100} values (inset) before and after a 20-h durability test. (f) Polarization curves of a two-electrode electrolyzer using cathode-anode combinations of B,N:Mo₂C@BCN-B, N:Mo₂C@BCN, and Pt/C-RuO₂@NF catalysts at a scanning rate of 2 mV/s and comparison of current densities at a cell voltage of 1.8 V before and after chronoamperometry (inset). (g) Electrolyzer stability test by chronoamperometry. (h) Pulse chronopotentiometric curve for H₂/O₂ evolution in a B,N:Mo₂C@BCN electrolyzer with the current density of $-10/10 \text{ mA}\cdot\text{cm}^{-2}$. The reversion time interval between the anode and cathode was 600 s in 1.0 M KOH solution. Reproduced with permission from [53]. Copyright 2018 American Chemical Society Catalysis.

3.6. MXene

MXene materials and their nanocomposites are considered emerging electrocatalysts for OER due to their high surface area, tunable electric structure, and thermal stability. They are a burgeoning class of 2D transition metal carbide or carbonitride nanosheets which are 3, 5, or 7 atomic layers thick and have some special properties compared to traditional 3D counterparts. Graphene is the most well-known 2D material with only a single atomic carbon layer, which leads to its limited use. Recently, MXene materials have gained great attention for the large variety of compositions, conductive property, and special morphology. A conventional synthesis method of MXenes is via selective etching of the 'A' elements in MAX phase precursors (general formula $M_{n+1}AX_n$, in which 'M' represents early transition metals; 'A' is a group A element mainly in IIIA and IVA; 'X' is carbon or nitrogen; and 'n' usually equals 1, 2, or 3, Figure 11) by hydrofluoric acid or fluoride (HF, NH₄HF₂, and so on) [40]. The other synthesis approaches include a high temperature method and CVD [103]. Meanwhile, method of etching from a non-MAX phase to form MXene has also been reported [104].

MXene materials are mainly used in supercapacitors and lithium-ion batteries. However, in recent years, researchers have gradually realized the merits of MXene as catalyst materials for OER, and they have achieved good results. For a long time, there had been a view that transition metal oxides displayed better catalytic activity than most TMCs. However, some MXene materials, which are stable

in aqueous media and immune to oxidation, show good practical application effect compared with transition metal oxides, which proves the potential advantages of TMCs [73]. The mainstream view is that the best strategy for maximizing the utilization of MXene is to use it as the substrate, which makes it easy to hybridize with other nano materials, so as to prepare electrocatalysts with higher catalytic activity.

One defect that limits the practical use of MXene materials is their tendency to intersheet aggregation driven by van der Waals force [105]. To solve this problem, freeze-drying, NPs forming, and polymer and hollow shell structures may be beneficial, but are restricted in large-scale production [106]. Xiu et al. [37] reported a hierarchical 3D architecture MXene material CoP@3D Ti₃C₂-MXene (Figure 10b) with high resistance towards aggregation. The capillary-forced strategy was utilized, which proved to be successful in forestalling aggregation between intersheets, and highly enhanced the electrochemical activity, thus accelerating the kinetic process. The synthesis method of CoP@3D Ti₃C₂-MXene is as follows: NPs of Co₃O₄ are dispersed on 3D architecture Ti₃C₂ MXene (produced by selectively etching Al from the Ti₃AlC₂ MAX phase with LiF/HCl), and the obtained product is then modulated via phosphorization at a high temperature to fabricate the CoP@3D Ti₃C₂-MXene material (Figure 10a).

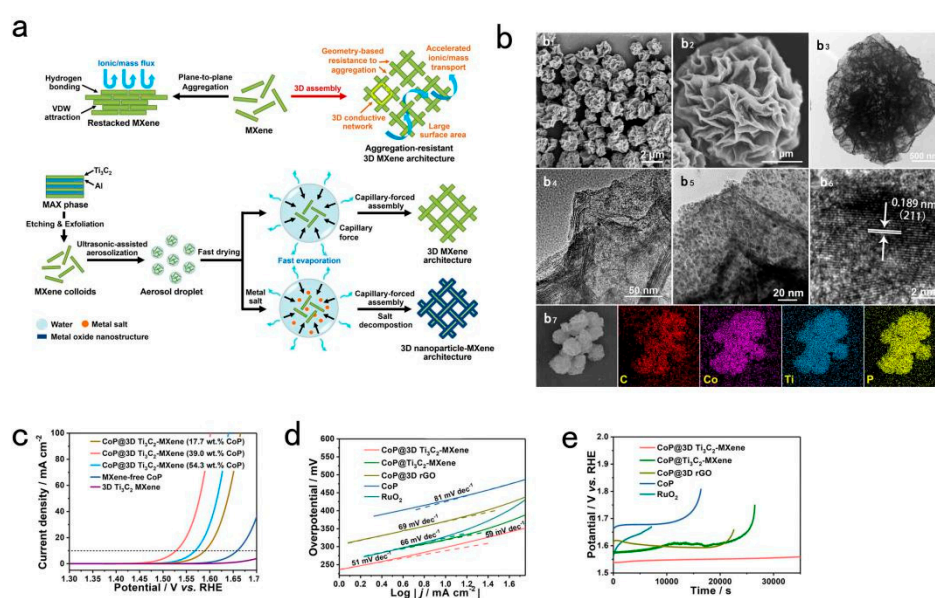


Figure 10. (a) Fabrication, hybridization, and advantages of the 3D MXene architecture. (b) Images, dispersion, and elements mapping of CoP@3D Ti₃C₂-MXene material. Figure (b₁,b₂) are the scanning electron microscopy (SEM) images of CoP@3D Ti₃C₂-MXene catalyst. Besides, Figure (b₃–b₅) exhibit the transmission electron microscopy (TEM) images of CoP@3D Ti₃C₂-MXene material, which demonstrate the dispersion of CoP NPs on the surface of 3D MXene. Figure (b₆) is the high resolution transmission electron microscopy (HRTEM) image of CoP NPs, which reveals the clear lattice fringes from the plane of CoP crystal and proves the single crystalline nature of CoP NPs. Figure (b₇) is the element mapping that displays the homogeneous scattering of C, Co, Ti, and P elements in the CoP@3D Ti₃C₂-MXene architecture. (c) The IR-corrected LSV, (d) Tafel plots, and (e) chronopotentiometric response at a current density of 10.0 mA·cm⁻² of CoP@3D Ti₃C₂-MXene, CoP@Ti₃C₂-MXene (different architecture), CoP@3D reduced graphene oxide (rGO), CoP, 3D Ti₃C₂ MXene (different hybridization), and RuO₂ (commercial catalyst) catalysts for OER in alkaline solution (1.0 M KOH). Reproduced with permission from [37]. Copyright 2018 American Chemical Society Nano.

Via electrochemical tests, the CoP@3D Ti₃C₂-MXene material displayed an overpotential ($\eta_{j=10}$) value of 220 to 340 mV vs. RHE, with a Tafel slope of 51 to 60 mV decade⁻¹ (changed with the proportion of added CoP), which outperformed commercial RuO₂ in identical conditions (Figure 10c,d). Additionally, this electrocatalyst exhibited a constant operating potential for 10 h (Figure 10e), which

demonstrated its superior durability. Surprisingly, CoP@3D Ti_3C_2 -MXene/CP, which was fabricated by loading carbon paper (CP) on a CoP@3D Ti_3C_2 -MXene catalyst, was a bifunctional electrocatalyst efficient for the overall water splitting reaction, proving that modulating the architecture of MXene, and/or coating other material on it to improve its electrocatalytic ability is possible. Similarly, another bifunctional MXene material reported by Le et al. [39] was synthesized by combining the known catalytic active phase IrCo with plane-porous Ti_3C_2 MXene (named IrCo@ac- Ti_3C_2). The as-fabricated electrocatalyst had an overpotential value of $\eta_{j=10} = 220$ mV, as shown in Figure 12a, with a long-term stability in 1.0 M KOH, thus it outweighed the activity of the other prepared catalysts in HER (displayed in Figure 12b).

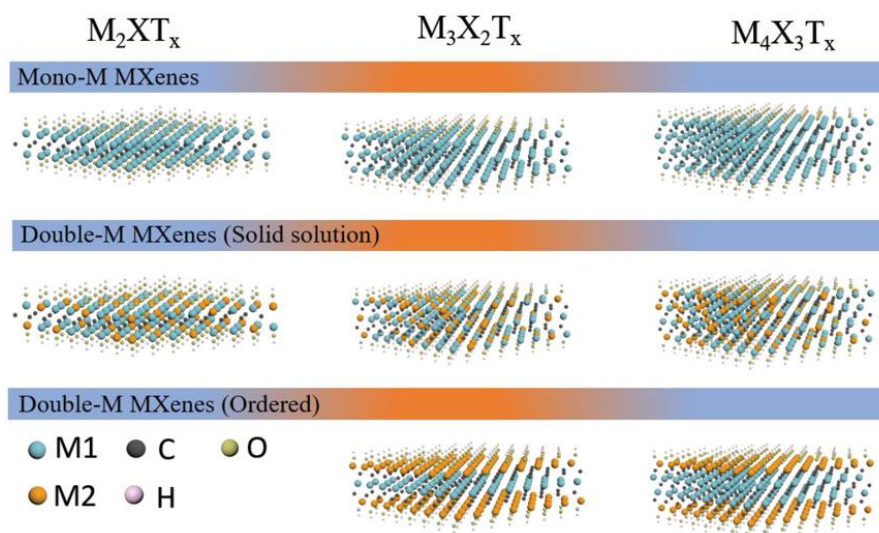


Figure 11. MXene materials have three different formulas (M_2XT_x , $\text{M}_3\text{X}_2\text{T}_x$, and $\text{M}_4\text{X}_3\text{T}_x$) and three different structures, including mono-M elements, solid solution double-M elements, and ordered double-M elements. In the ordered double-M elements MXene, one transition metal forms the peripheral layers, while the other occupies the central layer, whereas the solid solution double-M MXene has no sequence like this. Reproduced with permission from [40]. Copyright 2019 *Small*.

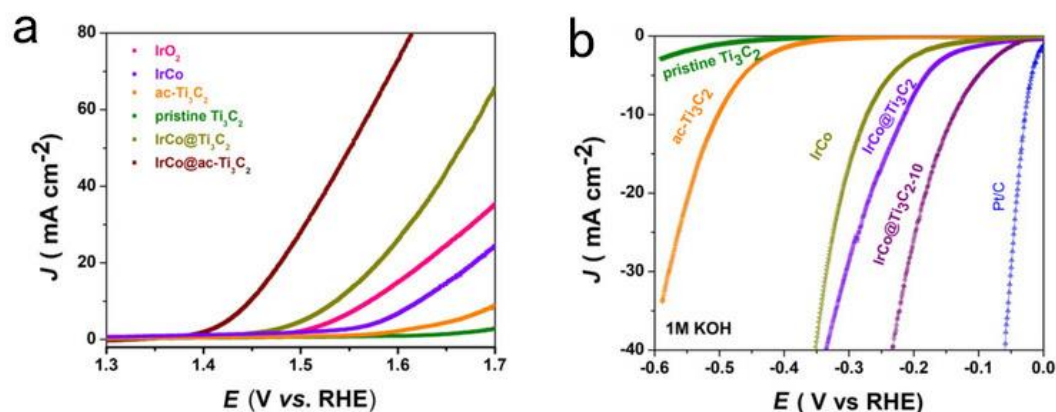


Figure 12. (a) OER and (b) HER IR-corrected polarization curves of IrCo@ac- Ti_3C_2 with a scan rate of 10 mV/s in 1.0 M KOH that demonstrate its bifunctional ability. Reproduced with permission from [39]. Copyright 2020 *ChemSusChem*.

The above two electrocatalysts demonstrate that some MXene compounds display superior performance for OER. Besides, the importance of material modification also lies in porosity engineering, which efficiently shortens the charge transmission passways and speeds up the kinetic process. More significantly, Ti_3C_2 MXene can be molded into various structures to enhance its conductivity,

which is expected meaningful for the future development of OER. For example, Michael et al. [107] reported a clay-shaped Ti_3C_2 MXene which could be dried into solid or rolled into films with extremely high volumetric capacitance of up to 900 farads per cube centimeter, and the property of this architecture is possibly suitable for OER. We have to indicate that plenty of TMCs with a high conductivity and porous quality have been proven to be efficient electrocatalysts for OER. Therefore, synthesis procedures with apt controlling might be beneficial for yielding ideal electrocatalysts, which gives eloquent proof of the importance of research on synthesis.

Graphene material has also been one of the most popular 2D catalysts in recent study. $\text{g-C}_3\text{N}_4$, as we mentioned in Section 3.4, originating from interaction between metal centers and an N-rich network [108], has similar morphology to MXene. In the study of Tian et al. [109], $\text{g-C}_3\text{N}_4$ was coupled with Ti_3C_2 MXene nanosheets to form a rich-surface area electrocatalyst (called TCCN) through Ti-N_x interaction. The TCCN film, which achieved an onset potential of 1.44 V and an $E_{j=10}$ magnitude of 1.65 V with a Tafel slope of 74.6 mV decade⁻¹ in 0.1 M KOH, exhibited a better OER catalytic activity than IrO_2/C . Notably, the freestanding TCCN film afforded a high double layer capacitance (C_{dl}) of 29.7 mF cm⁻², which outperformed the powdery TCCN (ball-milled film TCCN, $C_{dl} = 10.3 \text{ mF cm}^{-2}$), and revealed that the freestanding film structure was more effective in magnifying the active surface area, thus also demonstrating the superiority of MXene materials for OER from another perspective. As they noted, coupling different 2D materials to form hybrid catalysts through interactions between them is a worthwhile way of enhancing their electrocatalytic activity.

Coincidentally, another extensively researched material, named 2D MOF, with porous structure and fast electron transfer property, was also utilized to hybridize Ti_3C_2 MXene nanosheets, in order to achieve further improved OER performance [110,111]. Zhao et al. [41] focused on in situ hybridizing 2D cobalt 1,4-benzenedicarboxylate (CoBDC) with Ti_3C_2 MXene nanosheets through an interdiffusion reaction-assisted process (Figure 13a), the aim was to combine the porous structure (CoBDC MOF) and conductivity and hydrophilia character (Ti_3C_2 MXene nanosheets) to form a composite electrocatalyst, in order to facilitate the four-electron transfer process.

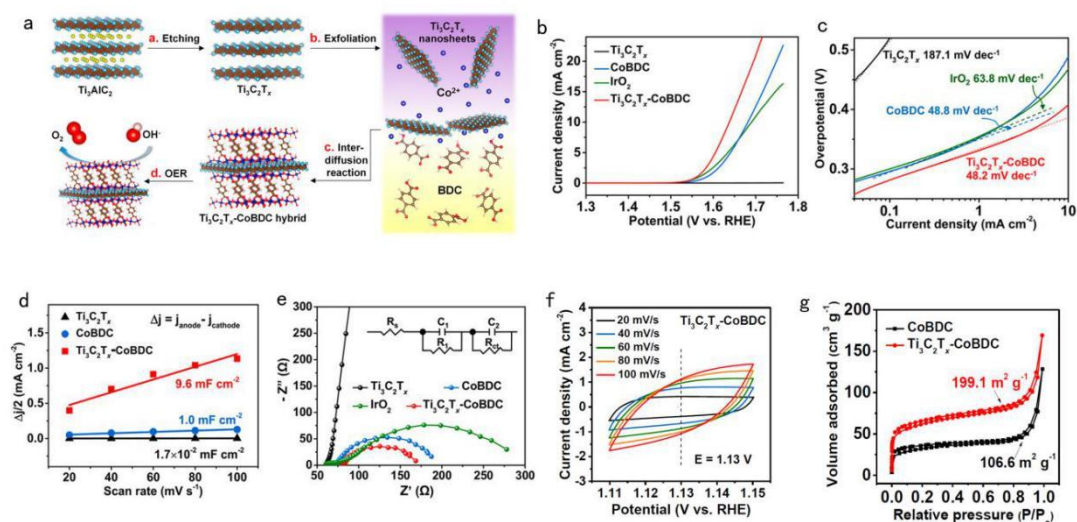


Figure 13. (a) Illustration of the hybridization procedures of Ti_3C_2 MXene nanosheets and a cobalt 1,4-benzenedicarboxylate (CoBDC) MOF. (b) LSV curves, (c) Tafel plots, and (d) C_{dl} of CoBDC, $\text{Ti}_3\text{C}_2\text{T}_x$, and $\text{Ti}_3\text{C}_2\text{T}_x\text{-CoBDC}$ hybrid. (e) Nyquist plots (EIS) of CoBDC, $\text{Ti}_3\text{C}_2\text{T}_x$, $\text{Ti}_3\text{C}_2\text{T}_x\text{-CoBDC}$ hybrid, and IrO_2 . (f) CV curves of $\text{Ti}_3\text{C}_2\text{T}_x\text{-CoBDC}$ hybrid at a scan rate of 20 to 100 mV/s at a potential range of 1.11 to 1.15 V vs. RHE without obvious Faradaic process. (g) The specific surface area of $\text{Ti}_3\text{C}_2\text{T}_x\text{-CoBDC}$ hybrid. Reproduced with permission from [41]. Copyright 2017 American Chemical Society Nano.

The $\text{Ti}_3\text{C}_2\text{T}_x$ -CoBDC hybrid material displayed a potential of 1.64 V vs. RHE and a Tafel slope of $48.2 \text{ mV decade}^{-1}$ at a current density of 10 mA/cm^2 in 0.1 M KOH (Figure 13b,c). As can be seen in Figure 13d,e, it also exhibited a higher double layer capacitance (9.6 mF/cm^2) and smaller semicircle region than its pure components, which was in good agreement with its high surface area of $199.1 \text{ m}^2 \text{ g}^{-1}$ (Figure 13g) caused by the porous morphology. Such a large surface area and high conductivity provided more active sites for the electron transfer process, therefore leading to an extraordinary OER efficiency. Moreover, the authors also pointed out that Ti_3C_2 MXene nanosheets might prevent the aggregation of CoBDC MOF, and thus put forward a new idea for tackling the problem of assembling intersheets of 2D materials. The work of above two groups suggest that combining diverse 2D catalysts may help to gather their desirable functional properties together to form an outstanding electrocatalyst for OER.

Except for Ti-based MXenes, we intend to introduce other 2D materials which have similar properties to MXenes as comparison to preferably analyse the intrinsic characters of these sorts of catalysts. Liang et al. [42] reported a single crystalline CoNiPS_3 incorporated with N-doped carbon nanosheets electrocatalyst (CoNiPS_3/C). This electrocatalyst formed a mosaic structure and exhibited an overpotential of 262 mV at $30 \text{ mA}\cdot\text{cm}^{-2}$ (Figure 16a,c), and a Tafel slope of $56 \text{ mV decade}^{-1}$ (Figure 16b) in a traditional three-electrode system in 1.0 M KOH . Furthermore, after being separated into CoNiPS_3/C nanodots, the electrocatalyst showed a much better catalytic ability; however, the stability was severely decreased (Figure 16d).

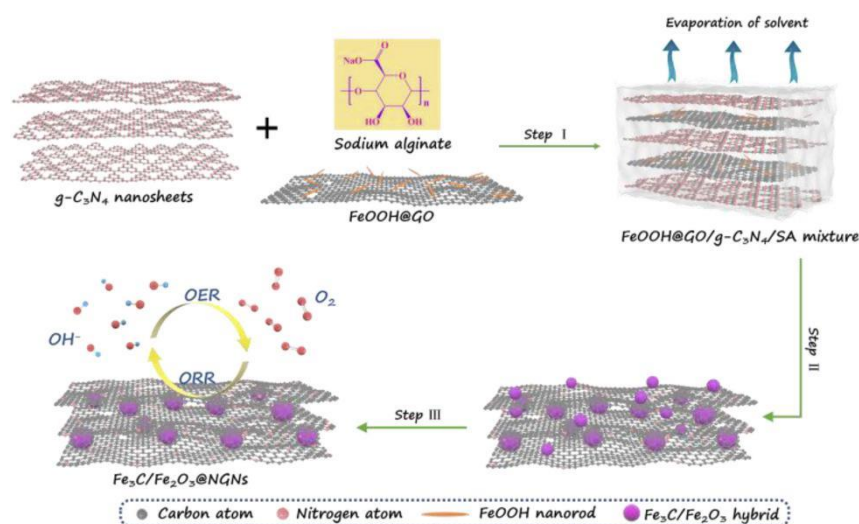


Figure 14. Synthesis method for $\text{Fe}_3\text{C}/\text{Fe}_2\text{O}_3@$ NGNs. Reproduced with permission from [43]. Copyright 2019 Carbon.

Since the first $\text{Ti}_3\text{C}_2\text{T}_x$ MXene has been successfully fabricated, it has developed rapidly based on its electrical and mechanical properties. However, the applications of exfoliated MXene material without appropriate surface morphology modification (denoted “bare MXene”) have rather limited further development [112]. Heterostructure and hybridization approaches for future prospects of MXene are of great importance. We also have to indicate that the hybridization and heterostructure modification methods of MXenes for OER are restricted to a specific form (MXene substrate) and Ti_3C_2 MXene phase are widely focalized, while the other kinds of MXenes have been less studied. For example, $\text{Pt}/\text{Nb}_2\text{CT}_x$ MXene material and its compounds have been reported beneficial for water-gas shift light alkane dehydrogenation [113]. Besides, Mo_2CT_x , which delivered an overpotential of 283 mV at $10 \text{ mA}\cdot\text{cm}^{-2}$ in $0.5 \text{ M H}_2\text{SO}_4$ for HER, also deserves more research [114].

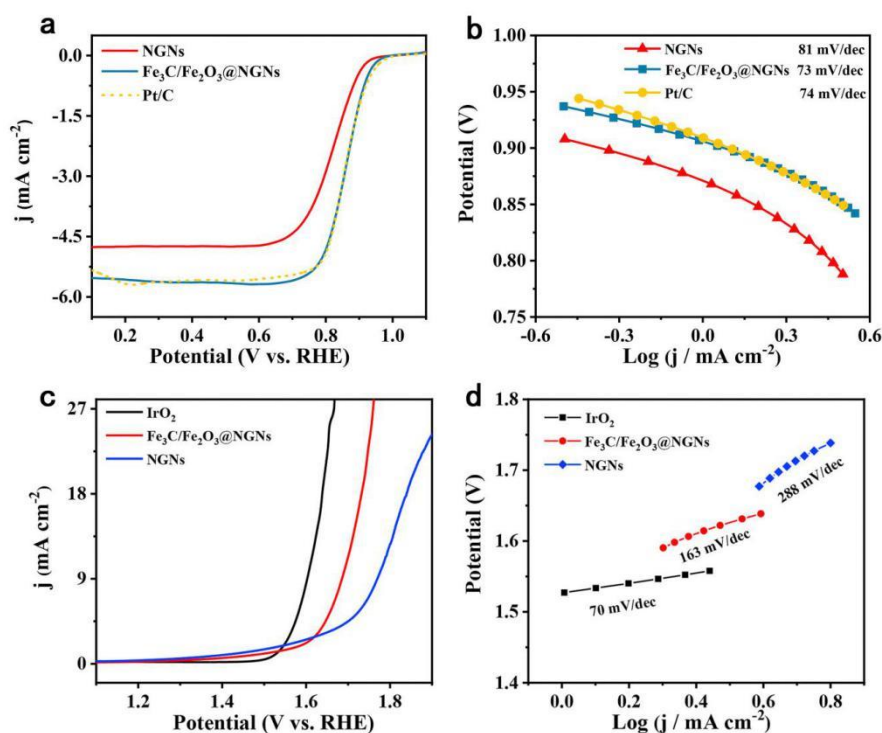


Figure 15. (a) ORR LSV curves of N-doped graphene (NGNs), Fe₃C/Fe₂O₃@NGNs, and commercial Pt/C electrocatalysts in O₂-saturated 0.1 M KOH condition. (b) The ORR Tafel plots of NGNs, Fe₃C/Fe₂O₃@NGNs, and Pt/C electrocatalysts obtained by fitting LSV curves using linear equation at 1600 rpm. (c) OER LSV curves of Fe₃C/Fe₂O₃@NGNs, NGNs and IrO₂ in N₂-saturated 0.1 M KOH. (d) The OER Tafel plots of Fe₃C/Fe₂O₃@NGNs, NGNs and IrO₂. Reproduced with permission from [43]. Copyright 2019 Carbon.

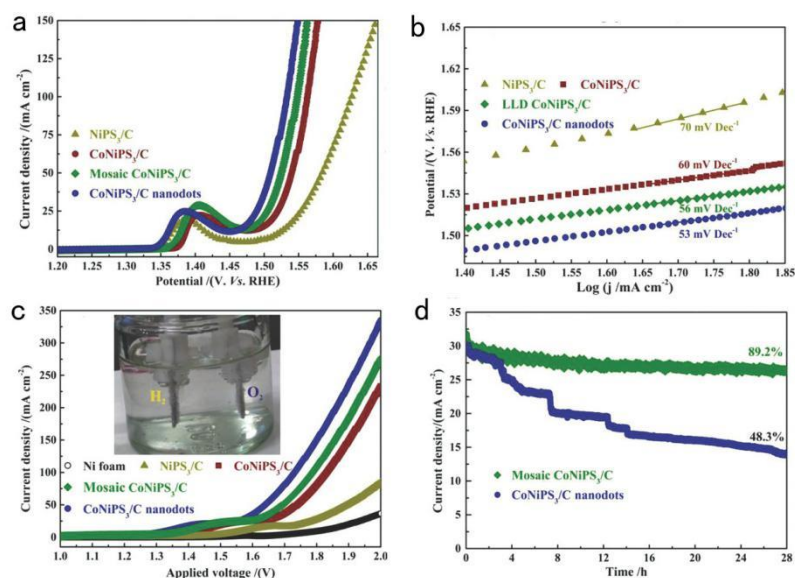


Figure 16. (a) OER curves, (b) Tafel plots, and (c) polarization curves of NiPS₃/C, CoNiPS₃/C, and the mosaic CoNiPS₃/C nanosheets and nanodots. The inset image in (c) shows the mosaic CoNiPS₃/C nanosheets used in water electrolysis. (d) Chronoamperometric curves of nanosheets and nanodots of CoNiPS₃/C. Reproduced with permission from [42]. Copyright 2018 Advanced Functional Materials.

Another important MXene material, 2D Mo₂C, which has recently attracted the attention of many researchers, displays promising prospects for HER. Geng et al. [115] successfully synthesized a 2D

Mo₂C-on-graphene film by means of molten copper-catalyzed CVD. In this material, nanometer-thin Mo₂C particles grow on the base of graphene and form a vertical heterostructure, which is an extremely excellent electrocatalyst for HER. The as-fabricated Mo₂C MXene displayed an overpotential of 236 mV vs. RHE at 10 mA/cm² and a Tafel slope of 73 mV dec⁻¹, and after 1000 CV cycles, no obvious decrease could be seen. However, despite the satisfactory performance of Mo₂C MXene for HER, the CVD synthesis method requires a high temperature to melt the metals, especially the most common catalyst of Cu, which severely wastes energy. Therefore, Chaitoglou et al. proposed a new low-temperature CVD method, by using a liquid Sn-Cu alloy as the catalyst. In this way, the temperature demand could be reduced to 880 °C, compared with the usual 1084 °C, and the cost of energy decreased without sacrificing the quality of the Mo₂C/graphene film. The electrocatalyst also exhibited a better result than the pure Mo₂C [116]. As the synthetic method has been developed, Mo₂C, which is proved to be an excellent catalyst for HER, might also become low-cost and efficient OER electrocatalyst.

The applications of MXenes are few in number on account of the lack of theoretical predictions and experiments [38], the utilization of unexplored MXene materials for OER is worth anticipating.

4. Conclusions and Future Perspectives

Searching for a newly-developing renewable energy system to replace traditional fossil fuels has recently been an essential task for fulfilling the progress of sustainable requirements. Simultaneously, converting new resources into storable energies is also one of the main objects of current research. Therefore, electrocatalysis for OER is of great significance as it provides us with the possibility to address both goals. To enhance the electrocatalysis efficiency, promising electrocatalysts undoubtedly play a critical role in OER system. In this review article, we have outlined fundamental understandings and experimental examples in the field of OER, the concepts of parameters, and measurement criteria for OER. Intrinsic properties, hybridization, and synthesis methods of different types of TMCs are emphasized. Additionally, the morphology, performance, and comparison with precious metal catalysts are proposed to evaluate the effects of recently fabricated TMCs, as well as their hybrids.

There has been great interest in TMC materials for OER because of their amazing catalytic abilities, including high conductivity, malleable property, abundant active sites, and stability. Moreover, their low cost and easy accessibility make them potential candidates for OER and other energy systems in the future. The major TMCs researched in OER field consist of MXene, Ni₃C, Fe₃C, Mo₂C, and WC, with various kinds of morphologies and useful characters, but similarly exhibit excellent activities as catalytic electrodes. TMCs are promising substrates and frameworks, through hybridization, coating, and combination with perovskite spinel and graphene families, their catalytic ability can be highly enhanced due to heterostructure and high electrochemical active sites for the charge transfer of kinetics. Some also exhibit amazing conductivity and can act as bifunctional catalysts, being beneficial for overall water splitting. Transition metal carbide compounds doped with foreign elements exhibit more efficient performance than the pure TMCs, indicating the vital importance of combinations for electrocatalysts. In a manner of speaking, these works have laid the foundation for the development of OER.

Although progress has been achieved, the drawbacks of TMC electrocatalysts are also evident. We have to point out that, compared with precious metals and traditional metal oxides, as catalysts, problems for TMCs are more difficult to address. Here, we put forward some issues that need to be tackled and potential research trends, respectively, as follows.

One of the most basic problems for TMC electrocatalysts for OER is that the mechanism is still debated and needs to be researched. Considering this reaction is under harsh oxidative condition, including the oxidation to the outer surface or inner core and the oxidation of both, the mechanism of which has not been investigated by DFT to date because the complexity caused by the oxides of catalytic materials as confirmed by Yang et al. [36]. Therefore, focusing on mechanism and kinetics in different conditions is of paramount necessity. It mostly depends on the development of advanced technology since they can indicate the accurate catalyst structure and thus helping to analyse the concrete

mechanism. Regarding this situation, in situ characterization techniques may help. For example, the in situ X-ray absorption spectroscopy (XAS) once used by Yang et al. [117] has recently become quite popular in OER mechanism research. Besides, Massel et al. [118] took advantage of in situ XAS and XRD to evaluate the active sites and mechanism of co-phosphate catalysts in solid fuels. Note that under existing experimental conditions, in situ characterization cannot be easily carried out, thus the research of kinetic process and reaction pathways deserve further study.

Secondly, the lack of large-scale fabrication techniques limits the pragmatic applications of TMCs as electrocatalysts for OER. As we have mentioned, the conventional synthesis methods—both the template-free and template-assisted one—require a high-temperature environment, which consumes excessive energy, so they are both unaffordable for industrial production. Herein, effective and energy-saving approaches for TMC synthesis are required, the development of which will certainly promote the applications of TMCs in many fields, particularly in OER. The long and sophisticated process of yielding pure and high-quality TMCs also sets a barrier for the improvement of TMCs. The properties of catalysts, which affect the performance for OER profoundly, depend on the crystalline structure. However, the orientation growth in the surface or inter-surface area of TMC materials is unpredictable and difficult to control. As a result, it takes an extremely long period of time to synthesize satisfying electrocatalysts, even if we already know the specific ideal structure. The situation asks for more accurate manipulation of synthesis process, which requires long-term research. Nevertheless, some hybridization and mosaic methods may help. For example, doping extraneous elements and/or changing the morphology in order to modify pure TMCs is one of the main ways of enhancing the material's catalytic ability. In addition, combining perovskite or graphene with the original electrocatalyst may have a large effect on the catalytic properties, which may result in high conductivity and more active sites in the catalyst and make it a promising catalyst. Other than this, another approach is to optimize the synthesis approach, or invent new ones, modulating dimensions and crystalline forms, such as 2D structure or nanostructure, in order to adapt to OER.

In short, whilst TMCs have recently been focused on, there is still only a small amount of research on them. We have to point out that TMC electrocatalysts deserve to be deeply explored due to their excellent performance for OER in the overall water splitting reaction and their low-cost property, which are very promising for the future compared with other materials. The development of highly active structures—such as MOF, graphene, and nano technology—will allow TMCs to exhibit varied possibilities. We believe that with the support of principles, theoretical mechanism, and experimental standpoints, applications for practical and large-scale use of TMCs as electrocatalysts for OER can be highly anticipated. Moreover, the advantages of TMCs will facilitate the development of other electrocatalytic systems as they share similar conditions and issues.

Author Contributions: Y.W. wrote the introduction, as well as Sections 2 and 3.6, in addition to carrying out revision work. Q.W. was responsible for the writing of Sections 3.1–3.3. L.T. finished Sections 3.4 and 3.5 and checked all the formats of references. B.Z. wrote the abstract and the conclusion and also revised the manuscript. Corresponding authors K.L. and X.Z. designed the whole work and revised the manuscript. Y.W., Q.W., B.Z. and L.T. share same contribution to this article. All authors have read and agreed to the published version of the manuscript.

Funding: This work was supported by Nankai University Undergraduate Innovation Projects 100 (no. 201910055811) and the State Key Laboratory of Simulation and Regulation of Water Cycle in River Basin (no. IWHR-SKLF201806).

Acknowledgments: This work was supported by Nankai University Undergraduate Innovation Projects 100 (no. 201910055811) and the State Key Laboratory of Simulation and Regulation of Water Cycle in River Basin (no. IWHR-SKLF201806).

Conflicts of Interest: There are no conflicts to declare.

References

1. Yan, X.D.; Tian, L.H.; He, M.; Chen, X.B. Three-dimensional crystalline/amorphous Co/Co₃O₄ core/shell nanosheets as efficient electrocatalysts for the hydrogen evolution reaction. *Nano Lett.* **2015**, *15*, 6015–6021. [[CrossRef](#)] [[PubMed](#)]
2. Yang, Y.; Fei, H.L.; Ruan, G.D.; Tour, J.M. Porous cobalt-based thin film as a bifunctional catalyst for hydrogen generation and oxygen generation. *Adv. Mater.* **2015**, *27*, 3175–3180. [[CrossRef](#)] [[PubMed](#)]
3. Jeong, D.; Jin, K.; Jerng, S.E.; Seo, H.; Kim, D.; Nahm, S.H.; Kim, S.H.; Nam, K.T. Mn₅O₈ nanoparticles as efficient water oxidation catalysts at neutral ipH. *ACS Catal.* **2015**, *5*, 4624–4628. [[CrossRef](#)]
4. Tang, C.; Wang, H.S.; Wang, H.F.; Zhang, Q.; Tian, G.L.; Nie, J.Q.; Wei, F. Spatially confined hybridization of nanometer-sized NiFe hydroxides into nitrogen-doped graphene frameworks leading to superior oxygen evolution reactivity. *Adv. Mater.* **2015**, *27*, 4516–4522. [[CrossRef](#)] [[PubMed](#)]
5. Ramesh, R.; Sawant, S.Y.; Nandi, D.K. Hydrogen Evolution Reaction by Atomic Layer-Deposited MoN_x on Porous Carbon Substrates: The Effects of Porosity and Annealing on Catalyst Activity and Stability. *ChemSusChem* **2020**, *13*, 4159–4168. [[CrossRef](#)]
6. Wu, P.W.; Wu, J.; Si, H.N. 3D Holey-Graphene Architecture Expedites Ion Transport Kinetics to Push the OER Performance. *Adv. Energy Mater.* **2020**, *10*, 2001005. [[CrossRef](#)]
7. Chen, B.T.; Morlanes, N.; Adogla, E.; Takanahe, K.; Rodionov, V.O. An efficient and stable hydrophobic molecular cobalt catalyst for water electro-oxidation at neutral pH. *ACS Catal.* **2016**, *6*, 4647–4652. [[CrossRef](#)]
8. Wang, J.; Zhong, H.X.; Wang, Z.L.; Meng, F.L.; Zhang, X.B. Integrated three-dimensional carbon paper/carbon tubes/cobalt-sulfide sheets as an efficient electrode for overall water splitting. *ACS Nano* **2016**, *10*, 2342–2348. [[CrossRef](#)]
9. Wang, H.; Hsu, Y.Y.; Chen, R.; Chan, T.S.; Chen, H.M.; Liu, B. Ni³⁺-induced formation of active NiOOH on the spinel Ni–Co oxide surface for efficient oxygen evolution reaction. *Adv. Energy Mater.* **2015**, *5*, 5. [[CrossRef](#)]
10. Tian, J.Q.; Liu, Q.; Asiri, A.M.; Sun, X.P. Self-supported nanoporous cobalt phosphide nanowire arrays: An efficient 3D hydrogen-evolving cathode over the wide range of pH 0–14. *J. Am. Chem. Soc.* **2014**, *136*, 7587–7590. [[CrossRef](#)]
11. Wu, Y.Z.; Chen, M.X.; Han, Y.Z.; Luo, H.X.; Su, X.J.; Zhang, M.T.; Lin, X.H.; Sun, J.L.; Wang, L.; Deng, L.; et al. Fast and simple preparation of iron-based thin films as highly efficient water-oxidation catalysts in neutral aqueous solution. *Angew. Chem.* **2015**, *127*, 4952–4957. [[CrossRef](#)]
12. Chen, P.Z.; Xu, K.; Fang, Z.W.; Tong, Y.; Wu, J.C.; Lu, X.L.; Peng, X.; Ding, H.; Wu, C.Z.; Xie, Y. Metallic Co₄N porous nanowire arrays activated by surface oxidation as electrocatalysts for the oxygen evolution reaction. *Angew. Chem. Int. Ed.* **2015**, *54*, 14710–14714. [[CrossRef](#)] [[PubMed](#)]
13. Tian, J.Q.; Liu, Q.; Cheng, N.Y.; Asiri, A.M.; Sun, X.P. Self-supported Cu₃P nanowire arrays as an integrated high-performance three-dimensional cathode for generating hydrogen from Water. *Angew. Chem. Int. Ed.* **2014**, *53*, 9577–9581. [[CrossRef](#)] [[PubMed](#)]
14. Bockris, J.O.M. Hydrogen economy in the future. *Int. J. Hydrogen Energy* **1999**, *24*, 1–15. [[CrossRef](#)]
15. Chen, Q.; Fu, Y.L.; Jin, J.L.; Zang, W.J.; Liu, X.; Zhang, X.Y.; Huang, W.Z.; Kou, Z.K.; Wang, J.; Zhou, L.; et al. In-situ surface self-reconstruction in ternary transition metal dichalcogenide nanorod arrays enables efficient electrocatalytic oxygen evolution. *J. Energy Chem.* **2021**, *55*, 10–16. [[CrossRef](#)]
16. Tang, Y.J.; Liu, C.H.; Huang, W. Bimetallic Carbides-Based Nanocomposite as Superior Electrocatalyst for Oxygen Evolution Reaction. *ACS Appl. Mater. Interfaces* **2017**, *9*, 16977–16985. [[CrossRef](#)] [[PubMed](#)]
17. Hu, Y.; Jensen, J.O.; Zhang, W. Hollow Spheres of Iron Carbide Nanoparticles Encased in Graphitic Layers as Oxygen Reduction Catalysts. *Angew. Chem. Int. Ed.* **2014**, *53*, 3675–3679. [[CrossRef](#)]
18. Benchakar, M.; Bilyk, T.; Garnero, C. MXene Supported Cobalt Layered Double Hydroxide Nanocrystals: Facile Synthesis Route for a Synergistic Oxygen Evolution Reaction Electrocatalyst. *Adv. Mater. Interfaces* **2019**, *6*, 1901328. [[CrossRef](#)]
19. Munir, A.; Haq, T.U.; Saleem, M.; Qurashi, A.; Hussain, S.Z.; Sher, F.; Hamid, A.U.; Jilani, A.; Hussain, I. Controlled engineering of nickel carbide induced N-enriched carbon nanotubes for hydrogen and oxygen evolution reactions in wide pH range. *Electrochim. Acta* **2020**, *341*, 136032. [[CrossRef](#)]

20. Li, G.L.; Zhang, X.B.; Zhang, H. Ultrathin 2D nanosheet based 3D hierarchical hollow polyhedral CoM/C (M = Ni, Cu, Mn) phosphide nanocages as superior electrocatalysts toward oxygen evolution reaction. *Chem. Eng. J.* **2020**, *398*, 125467. [[CrossRef](#)]
21. Ren, S.S.; Duan, X.D.; Ge, F.Y. Trimetal-based N-doped carbon nanotubes arrays on Ni foams as self-supported electrodes for hydrogen/oxygen evolution reactions and water splitting. *J. Power Sources* **2020**, *480*, 228866. [[CrossRef](#)]
22. Wang, H.P.; Zhu, S.; Deng, J.W.; Zhang, W.C.; Feng, Y.Z.; Ma, J.M. Transition metal carbides in electrocatalytic oxygen evolution reaction. *Chin. Chem. Lett.* **2020**. [[CrossRef](#)]
23. McCrory, C.C.L.; Jung, S.; Ferrer, I.M.; Chatman, S.M.; Peters, J.C.; Jaramillo, T.F. Benchmarking Hydrogen Evolving Reaction and Oxygen Evolving Reaction Electrocatalysts for Solar Water Splitting Devices. *J. Am. Chem. Soc.* **2015**, *137*, 4347–4357. [[CrossRef](#)] [[PubMed](#)]
24. Suen, N.T.; Hung, S.F.; Quan, Q. Electrocatalysis for the oxygen evolution reaction: Recent development and future perspectives. *Chem. Soc. Rev.* **2017**, *46*, 337–365. [[CrossRef](#)]
25. Yu, P.; Wang, F.M.; Shifa, T.A.; Zhan, X.Y.; Lou, X.D.; Xia, F.; He, J. Earth abundant materials beyond transition metal dichalcogenides: A focus on electrocatalyzing hydrogen evolution reaction. *Nano Energy* **2019**, *58*, 244–276. [[CrossRef](#)]
26. You, B.; Jiang, N.; Sheng, M.L.; Gul, S.; Yano, J.; Sun, Y.J. High-Performance Overall Water Splitting Electrocatalysts Derived from Cobalt-Based Metal–Organic Frameworks. *Chem. Mater.* **2015**, *27*, 7636–7642. [[CrossRef](#)]
27. Fei, H.L.; Dong, J.; Arellano-Jiménez, M.J. Atomic cobalt on nitrogen-doped graphene for hydrogen generation. *Nat. Commun.* **2015**, *6*, 8668. [[CrossRef](#)]
28. Zhang, Y.; Lu, T.; Ye, Y.K.; Dai, W.J.; Zhu, Y.A.; Pan, Y. Stabilizing Oxygen Vacancy in Entropy-Engineered CoFe₂O₄-Type Catalysts for Co-prosperity of Efficiency and Stability in an Oxygen Evolution Reaction. *ACS Appl. Mater. Interfaces* **2020**, *12*, 32548–32555. [[CrossRef](#)]
29. Frydendal, R.; Paoli, E.A.; Knudsen, B.P.; Wickman, B.; Malacrida, P.; Stephens, I.E.L.; Chorkendorff, I. Benchmarking the Stability of Oxygen Evolution Reaction Catalysts: The Importance of Monitoring Mass Losses. *ChemElectroChem* **2014**, *1*, 2075–2081. [[CrossRef](#)]
30. Yu, Y.; Zhou, J.; Sun, Z. Novel 2D Transition-Metal Carbides: Ultrahigh Performance Electrocatalysts for Overall Water Splitting and Oxygen Reduction. *Adv. Funct. Mater.* **2020**, 2000570. [[CrossRef](#)]
31. Anurupa, M. Cobalt-based heterogeneous catalysts in an electrolyzer system for sustainable energy storage. *Dalton Trans.* **2020**, *49*, 11430–11450.
32. Cheng, W.; Lu, X.F.; Luan, D.; Lou, X.W. NiMn-Based Bimetal–Organic Framework Nanosheets Supported on Multi-Channel Carbon Fibers for Efficient Oxygen Electrocatalysis. *Angew. Chem. Int. Ed.* **2020**, *59*, 18234–18239. [[CrossRef](#)] [[PubMed](#)]
33. Ouyang, T.; Ye, Y.Q.; Wu, C.Y.; Xiao, K.; Liu, Z.Q. Heterostructures Composed of N-Doped Carbon Nanotubes Encapsulating Cobalt and b-Mo₂C Nanoparticles as Bifunctional Electrodes for Water Splitting. *Angew. Chem. Int. Ed.* **2019**, *58*, 4923–4928. [[CrossRef](#)] [[PubMed](#)]
34. Wang, P.; Qin, R.; Ji, P.; Pu, Z.; Zhu, J.; Lin, C.; Zhao, Y.; Tang, H.; Li, W.; Mu, S. Synergistic Coupling of Ni Nanoparticles with Ni₃C Nanosheets for Highly Efficient Overall Water Splitting. *Small* **2020**, *16*, 2001642. [[CrossRef](#)] [[PubMed](#)]
35. Liu, Y.; Zhang, J.; Li, Y. Manipulating dehydrogenation kinetics through dual-doping Co₃N electrode enables highly efficient hydrazine oxidation assisting self-powered H₂ production. *Nat. Commun.* **2020**, *11*, 5148–5180. [[CrossRef](#)] [[PubMed](#)]
36. Yang, C.C.; Zai, S.F.; Zhou, Y.T.; Du, L.; Jiang, Q. Fe₃C-Co Nanoparticles Encapsulated in a Hierarchical Structure of N-Doped Carbon as a Multifunctional Electrocatalyst for ORR, OER, and HER. *Adv. Funct. Mater.* **2019**, *29*, 1901949. [[CrossRef](#)]
37. Xiu, L.Y.; Wang, Z.Y.; Yu, M.Z.; Wu, X.H.; Qiu, J.S. Aggregation-Resistant 3D MXene-Based Architecture as Efficient Bifunctional Electrocatalyst for Overall Water Splitting. *ACS Nano* **2018**, *12*, 8017–8028. [[CrossRef](#)]
38. Du, C.F.; Dinh, K.N.; Liang, Q.; Zheng, Y.; Luo, Y.; Zhang, J.; Yan, Q. Self-Assemble and In Situ Formation of Ni_{1-x}Fe_xPS₃ Nanomosaic-Decorated MXene Hybrids for Overall Water Splitting. *Adv. Energy Mater.* **2018**, *8*, 1801127. [[CrossRef](#)]

39. Anh, L.T.; Quang, T.N.; Yeseul, H.; Meeree, K.; Hyoyoung, L. Porosity-Engineering of MXene as a Support Material for a Highly Efficient Electrocatalyst toward Overall Water Splitting. *ChemSusChem* **2020**, *13*, 945–955.
40. Li, Z.; Wu, Y. 2D Early Transition Metal Carbides (MXenes) for Catalysis. *Small* **2019**, *15*, 15. [[CrossRef](#)]
41. Zhao, L.; Dong, B.; Li, S. Interdiffusion Reaction-Assisted Hybridization of Two-Dimensional Metal–Organic Frameworks and $\text{Ti}_3\text{C}_2\text{T}_x$ Nanosheets for Electrocatalytic Oxygen Evolution. *ACS Nano* **2017**, *11*, 5800–5807. [[CrossRef](#)] [[PubMed](#)]
42. Liang, Q.H.; Zhong, L.X.; Du, C.F.; Zheng, Y.; Luo, Y.B.; Xu, J.W.; Li, S.Z.; Yan, Q.Y. Mosaic-Structured Cobalt Nickel Thiophosphate Nanosheets Incorporated N-doped Carbon for Efficient and Stable Electrocatalytic Water Splitting. *Adv. Funct. Mater.* **2018**, *28*, 1805075. [[CrossRef](#)]
43. Tian, Y.H.; Xu, L.; Qian, J.C.; Bao, J.Y. $\text{Fe}_3\text{C}/\text{Fe}_2\text{O}_3$ heterostructure embedded in N-doped graphene as a bifunctional catalyst for quasi-solid-state zinc-air batteries. *Carbon* **2019**, *146*, 763–771. [[CrossRef](#)]
44. Zhao, P.P.; Hua, X.; Xu, W.; Luo, W.; Chen, S.L.; Cheng, G.Z. Metal–organic framework-derived hybrid of Fe_3C nanorod-encapsulated, N-doped CNTs on porous carbon sheets for highly efficient oxygen reduction and water oxidation. *Catal. Sci. Technol.* **2016**, *6*, 6365–6371. [[CrossRef](#)]
45. Fan, H.S.; Yu, H.; Zhang, Y.F.; Zheng, Y.; Dai, Z.F.; Li, B.; Zong, Y. Fe-Doped Ni_3C Nanodots in N-Doped Carbon Nanosheets for Efficient Hydrogen-Evolution and Oxygen-Evolution Electrocatalysis. *Angew. Chem. Int. Ed.* **2017**, *56*, 12566–12570. [[CrossRef](#)]
46. Geng, S.; Yang, W.W.; Yu, Y.S. Fabrication of $\text{NiC}/\text{MoC}/\text{NiMoO}_4$ Heterostructured Nanorod Arrays as Stable Bifunctional Electrocatalysts for Efficient Overall Water Splitting. *Chem. Asian J.* **2019**, *14*, 1013–1020. [[CrossRef](#)]
47. He, P.; Yu, X.Y.; Lou, X.W.D. Carbon-Incorporated Nickel-Cobalt Mixed Metal Phosphide Nanoboxes with Enhanced Electrocatalytic Activity for Oxygen Evolution. *Angew. Chem. Int. Ed.* **2017**, *56*, 3897–3900. [[CrossRef](#)]
48. Yang, H.; Luo, S.; Li, X. Controllable orientation-dependent crystal growth of high-index faceted dendritic $\text{NiC}_{0.2}$ nanosheets as high-performance bifunctional electrocatalysts for overall water splitting. *J. Mater. Chem. A* **2016**, *4*, 18499–18508. [[CrossRef](#)]
49. Joy, J.; Sekar, A.; Vijayaraghavan, S.; Kumar, P.; Pillai, V.K.; Alwarappan, S. Nickel-Incorporated, Nitrogen-Doped Graphene Nanoribbons as Efficient Electrocatalysts for Oxygen Evolution Reaction. *J. Electrochem. Soc.* **2018**, *165*, H141–H146. [[CrossRef](#)]
50. Regmi, Y.N.; Wan, C.; Duffee, K.D.; Leonard, B.M. Nanocrystalline Mo_2C as a Bifunctional Water Splitting Electrocatalyst. *ChemCatChem* **2015**, *7*, 3911–3915. [[CrossRef](#)]
51. Wang, H.; Cao, Y.J.; Sun, C.; Zou, G.F.; Huang, J.W.; Kuai, X.X.; Zhao, J.Q.; Gao, L.J. Strongly Coupled Molybdenum Carbide on Carbon Sheets as a Bifunctional Electrocatalyst for Overall Water Splitting. *ChemSusChem* **2017**, *10*, 3540–3546. [[CrossRef](#)] [[PubMed](#)]
52. Das, D.; Santra, S.; Nanda, K.K. In Situ Fabrication of a Nickel/Molybdenum Carbide-Anchored N-Doped Graphene/CNT Hybrid: An Efficient (Pre)catalyst for OER and HER. *ACS Appl. Mater. Interfaces* **2018**, *10*, 35025–35038. [[CrossRef](#)] [[PubMed](#)]
53. Raza, A.M.A.; Hee, L.M.; Sung, L.J. Boron- and Nitrogen-Codoped Molybdenum Carbide Nanoparticles Imbedded in a BCN Network as a Bifunctional Electrocatalyst for Hydrogen and Oxygen Evolution Reactions. *ACS Catal.* **2018**, *8*, 8296–8305.
54. Zhao, Y.X.; Bowers, C.W.; Spain, I.L. Graphitic nature of chemical vapor-deposited carbon filaments grown on silicon surfaces from acetylene. *Carbon* **1988**, *26*, 291–293. [[CrossRef](#)]
55. Fadil, N.A.; Saravanna, G.; Ramesh, G.V. Synthesis and electrocatalytic performance of atomically ordered nickel carbide (Ni_3C) nanoparticles. *Chem. Commun.* **2014**, *50*, 6451–6453. [[CrossRef](#)]
56. Wan, C.; Leonard, B.M. Iron-Doped Molybdenum Carbide Catalyst with High Activity and Stability for the Hydrogen Evolution Reaction. *Chem. Mater.* **2015**, *27*, 4281–4288. [[CrossRef](#)]
57. Hao, J.; Zhang, G.F.; Zheng, Y.T.; Luo, W.H.; Jin, C.; Wang, R.; Wang, Z.; Zheng, W.J. Controlled synthesis of Ni_3C /nitrogen-doped carbon nanoflakes for efficient oxygen evolution. *Electrochim. Acta* **2019**, *320*. [[CrossRef](#)]
58. Kang, J.; Duan, X.G.; Wang, C.; Sun, H.Q.; Tan, X.Y.; Tade, M.O.; Wang, S.B. Nitrogen-doped bamboo-like carbon nanotubes with Ni encapsulation for persulfate activation to remove emerging contaminants with excellent catalytic stability. *Chem. Eng. J.* **2018**, *332*, 398–408. [[CrossRef](#)]

59. Qin, Q.; Hao, J.; Zheng, W.J. Ni/Ni₃C Core/Shell Hierarchical Nanospheres with Enhanced Electrocatalytic Activity for Water Oxidation. *ACS Appl. Mater. Interfaces* **2018**, *10*, 17827–17834. [[CrossRef](#)]
60. Zi, Y.Y.; Yu, D.; Min, R.G. A one-dimensional porous carbon-supported Ni/Mo₂C dual catalyst for efficient water splitting. *Chem. Sci.* **2017**, *8*, 968–973.
61. Rostami, S.; Pour, A.N.; Salimi, A.; Abolghasempour, A. Hydrogen adsorption in metal-organic frameworks (MOFs): Effects of adsorbent architecture. *Int. J. Hydrogen Energy* **2018**, *43*, 7072–7080. [[CrossRef](#)]
62. Lee, J.Y.; Farha, O.K.; Roberts, J. Metal-organic framework materials as catalysts. *Chem. Soc. Rev.* **2019**, *38*, 1450–1459. [[CrossRef](#)] [[PubMed](#)]
63. Zhao, S.S.; Liu, Y.Y. Fluorescent Aromatic Tag-Functionalized MOFs for Highly Selective Sensing of Metal Ions and Small Organic Molecules. *Inorg. Chem.* **2016**, *55*, 2261–2273. [[CrossRef](#)] [[PubMed](#)]
64. Jia, X.X.; Wang, M.H.; Liu, G. Mixed-metal MOF-derived Co-doped Ni₃C/Ni NPs embedded in carbon matrix as an efficient electrocatalyst for oxygen evolution reaction. *Int. J. Hydrogen Energy* **2019**, *44*, 24572–24579. [[CrossRef](#)]
65. Levy, R.B.; Boudart, M. Platinum-Like Behavior of Tungsten Carbide in Surface Catalysis. *Science* **1973**, *181*, 547–549. [[CrossRef](#)]
66. Glibin, V.; Svirko, R.; Bashtan-Kandybovich, R. Synthesis, surface chemistry and electrocatalytic properties of oxygen-modified tungsten carbide in relation to the electrochemical hydrogen oxidation. *Surf. Sci.* **2010**, *604*, 500–507. [[CrossRef](#)]
67. Palanker, V.S.; Gajyev, R. On adsorption and electro-oxidation of some compounds on tungsten carbide; their effect on hydrogen electro-oxidation. *Electrochim. Acta* **1977**, *22*, 133–136. [[CrossRef](#)]
68. Zhou, X.S.; Qiu, Y.J. Tungsten carbide nanofibers prepared by electrospinning with high electrocatalytic activity for oxygen reduction. *Int. J. Hydrogen Energy* **2011**, *36*, 7398–7404. [[CrossRef](#)]
69. Han, N.; Yang, K.R.; Lu, Z. Nitrogen-doped tungsten carbide nanoarray as an efficient bifunctional electrocatalyst for water splitting in acid. *Nat. Commun.* **2018**, *9*, 924. [[CrossRef](#)]
70. Bukola, S.; Merzougui, B.; Akinpelu, A.; Zeama, M. Cobalt and Nitrogen Co-Doped Tungsten Carbide Catalyst for Oxygen Reduction and Hydrogen Evolution Reactions. *Electrochim. Acta* **2016**, *190*, 1113–1123. [[CrossRef](#)]
71. Kim, D.W.; Li, O.L.; Pootawang, P. Solution plasma synthesis process of tungsten carbide on N-doped carbon nanocomposite with enhanced catalytic ORR activity and durability. *RSC Adv.* **2014**, *4*, 16813–16819. [[CrossRef](#)]
72. Zhao, T.; Gao, J.K.; Wu, J.; He, P.P.; Li, Y.W.; Yao, J.M. Highly Active Cobalt/Tungsten Carbide@N-Doped Porous Carbon Nanomaterials Derived from Metal-Organic Frameworks as Bifunctional Catalysts for Overall Water Splitting. *Energy Technol.* **2019**, *7*, 1800969. [[CrossRef](#)]
73. Zhong, Y.; Xia, X.H.; Shi, F.; Zhan, J.Y.; Tu, J.P.; Fan, H.J. Transition Metal Carbides and Nitrides in Energy Storage and Conversion. *Adv. Sci.* **2016**, *3*, 1500286. [[CrossRef](#)] [[PubMed](#)]
74. Chen, J.G. Carbide and Nitride Overlayers on Early Transition Metal Surfaces: Preparation, Characterization, and Reactivities. *Chem. Rev.* **1996**, *96*, 1477–1498. [[CrossRef](#)]
75. Amiin, I.S.; Pu, Z.; Liu, X. Multifunctional Mo-N/C@MoS₂ Electrocatalysts for HER, OER, ORR, and Zn-Air Batteries. *Adv. Funct. Mater.* **2017**, *27*, 1702300. [[CrossRef](#)]
76. Qian, Y.H.; Hu, Z.G.; Ge, X.M.; Yang, S.L.; Peng, Y.W.; Kang, Z.X.; Liu, Z.L.; Lee, J.Y.; Zhao, D. A metal-free ORR/OER bifunctional electrocatalyst derived from metal-organic frameworks for rechargeable Zn-Air batteries. *Carbon* **2017**, *111*, 641–650. [[CrossRef](#)]
77. Jiang, H.; Gu, J.X.; Zheng, X.S.; Liu, M.; Qiu, X.Q. Defect-rich and ultrathin N doped carbon nanosheets as advanced trifunctional metal-free electrocatalysts for the ORR, OER and HER. *Energy Environ. Sci.* **2019**, *12*, 322–333. [[CrossRef](#)]
78. Arico, A.S.; Bruce, P.; Scrosati, B.; Tarascon, J.M.; Schalkwijk, W.V. Nanostructured materials for advanced energy conversion and storage devices. *Nat. Mater.* **2005**, *4*, 366–377. [[CrossRef](#)]
79. Debe, M.K. Electrocatalyst Approaches and Challenges for Automotive Fuel cells. *Nature* **2012**, *486*, 43–51. [[CrossRef](#)]
80. Fu, J.; Cano, Z.P.; Park, M.G.; Yu, A.P.; Fowler, M.; Chen, Z.W. Electrically Rechargeable Zinc-Air Batteries: Progress, Challenges, and Perspectives. *Adv. Mater.* **2017**, *29*, 1604685. [[CrossRef](#)]
81. Wang, Z.L.; Xu, D.; Xu, J.J.; Zhang, X.B. Oxygen electrocatalysts in metal-air batteries: From aqueous to nonaqueous electrolytes. *Chem. Soc. Rev.* **2014**, *43*, 7746–7786. [[CrossRef](#)] [[PubMed](#)]

82. Defilippi, C.; Shinde, D.V.; Dang, Z.; Manna, L.; Hardacre, C.; Greer, A.J.; D'Agostino, C.; Giordano, C. HfN Nanoparticles: An Unexplored Catalyst for the Electrocatalytic Oxygen Evolution Reaction. *Angew. Chem.* **2019**, *131*, 15610–15616. [[CrossRef](#)]
83. Song, J.Y.; Ren, Y.R.; Li, J.S.; Huang, X.B.; Cheng, F.Y.; Tang, Y.G.; Wang, H.Y. Coreshell Co/CoNx@C nanoparticles enfolded by Co-N doped carbon nanosheets as a highly efficient electrocatalyst for oxygen reduction reaction. *Carbon* **2018**, *138*, 300–308. [[CrossRef](#)]
84. Wu, Y.X.; Wang, T.H.; Zhang, Y.D.; Xin, S.; He, X.J.; Zhang, D.W.; Shui, J.L. Electrocatalytic performances of g-C₃N₄-LaNiO₃ composite as bi-functional catalysts for lithium-oxygen batteries. *Sci. Rep.* **2016**, *6*, 24314. [[CrossRef](#)] [[PubMed](#)]
85. Xu, C.Y.; Han, Q.; Zhao, Y.; Wang, L.X.; Li, Y.; Qu, L.T. Sulfur-doped graphitic carbon nitride decorated with graphene quantum dots for an efficient metal-free electrocatalyst. *J. Mater. Chem.* **2015**, *3*, 1841–1846. [[CrossRef](#)]
86. Wang, Q.C.; Lei, Y.P.; Chen, Z.Y. Fe/Fe₃C@C nanoparticles encapsulated in N-doped graphene–CNTs framework as an efficient bifunctional oxygen electrocatalyst for robust rechargeable Zn–air batteries. *J. Mater. Chem. A* **2017**, *6*, 516–526. [[CrossRef](#)]
87. Wu, N.; Lei, Y.P.; Wang, Q.C.; Wang, B.; Han, C.; Wang, Y.D. Facile synthesis of FeCo@NC core–shell nanospheres supported on graphene as an efficient bifunctional oxygen electrocatalyst. *Nano Res.* **2017**, *10*, 2332–2343. [[CrossRef](#)]
88. Su, C.Y.; Cheng, H.; Li, W.; Liu, Z.Q.; Li, N.; Hou, Z.; Bai, F.Q.; Zhang, H.X.; Ma, T.Y. Atomic Modulation of FeCo-Nitrogen-Carbon Bifunctional Oxygen Electrodes for Rechargeable and Flexible All-Solid-State Zinc-Air Battery. *Adv. Energy Mater.* **2017**, *7*, 1602420. [[CrossRef](#)]
89. Liu, Q.; Wang, Y.B.; Dai, L.M.; Yao, J.N. Scalable Fabrication of Nanoporous Carbon Fiber Films as Bifunctional Catalytic Electrodes for Flexible Zn–Air Batteries. *Adv. Mater.* **2016**, *28*, 3000–3006. [[CrossRef](#)]
90. Cui, Z.M.; Li, Y.T.; Fu, G.T. Robust Fe₃Mo₃C Supported IrMn Clusters as Highly Efficient Bifunctional Air Electrode for Metal–Air Battery. *Adv. Mater.* **2017**, *29*, 1702385. [[CrossRef](#)]
91. Chen, W.F.; Wang, C.H.; Sasaki, K. Highly active and durable nanostructured molybdenum carbide electrocatalysts for hydrogen production. *Energy Environ. Sci.* **2013**, *6*, 943–951. [[CrossRef](#)]
92. Liao, L.; Wang, S.N.; Xiao, J.J. A nanoporous molybdenum carbide nanowire as an electrocatalyst for hydrogen evolution reaction. *Energy Environ. Sci.* **2014**, *7*, 387–392. [[CrossRef](#)]
93. Wu, H.B.; Xia, B.Y.; Yu, L. Porous molybdenum carbide nano-octahedrons synthesized via confined carburization in metal-organic frameworks for efficient hydrogen production. *Nat. Commun.* **2015**, *6*, 6512. [[CrossRef](#)] [[PubMed](#)]
94. Regmi, Y.N.; Waetzig, G.R.; Duffee, K.D.; Schmuckler, S.M.; Thode, J.M.; Leonard, B.M. Carbides of group IVA, VA and VIA transition metals as alternative HER and ORR catalysts and support materials. *J. Mater. Chem. A* **2015**, *3*, 10085–10091. [[CrossRef](#)]
95. Zhu, J.; Holmen, A.; Chen, D. Carbon Nanomaterials in Catalysis: Proton Affinity, Chemical and Electronic Properties, and their Catalytic Consequences. *ChemCatChem* **2013**, *5*, 378–401. [[CrossRef](#)]
96. Chen, C.C.; Lin, C.L.; Chen, L.C. Functionalized Carbon Nanomaterial Supported Palladium Nano-Catalysts for Electrocatalytic Glucose Oxidation Reaction. *Electrochim. Acta* **2015**, *152*, 408–416. [[CrossRef](#)]
97. Zhao, Z.; Xia, Z. Design Principles for Dual-Element-Doped Carbon Nanomaterials as Efficient Bifunctional Catalysts for Oxygen Reduction and Evolution Reactions. *ACS Catal.* **2016**, *6*, 1553–1558. [[CrossRef](#)]
98. Podyacheva, O.Y.; Ismagilov, Z.R. Nitrogen-doped carbon nanomaterials: To the mechanism of growth, electrical conductivity and application in catalysis. *Catal. Today* **2015**, *249*, 12–22. [[CrossRef](#)]
99. Kim, M.; Kim, S.; Song, D.; Oh, S.; Chang, K.J.; Cho, E. Promotion of electrochemical oxygen evolution reaction by chemical coupling of cobalt to molybdenum carbide. *Appl. Catal. B Environ.* **2018**, *227*, 340–348. [[CrossRef](#)]
100. Jiang, J.; Liu, Q.; Zeng, C. Cobalt/molybdenum carbide@N-doped carbon as a bifunctional electrocatalyst for hydrogen and oxygen evolution reactions. *J. Mater. Chem. A* **2017**, *5*, 16929–16935. [[CrossRef](#)]
101. Dutta, S.; Indra, A.; Han, H.S. An Intriguing Pea-Like Nanostructure of Cobalt Phosphide on Molybdenum Carbide Incorporated Nitrogen-Doped Carbon Nanosheets for Efficient Electrochemical Water Splitting. *ChemSusChem* **2018**, *11*, 3956–3964. [[CrossRef](#)] [[PubMed](#)]
102. Zhu, X.; Zhang, X.; Huang, L. Cobalt doped beta-molybdenum carbide nanoparticles encapsulated within nitrogen-doped carbon for oxygen evolution. *Chem. Commun.* **2019**, *55*, 9995–9998. [[CrossRef](#)] [[PubMed](#)]

103. Xu, C.; Wang, L.B.; Liu, Z.B.; Chen, L.; Guo, J.K.; Kang, N.; Xiu, L.M.; Cheng, H.M.; Ren, W.C. Large-area high-quality 2D ultrathin Mo₂C superconducting crystals. *Nat. Mater.* **2015**, *14*, 1135–1141. [[CrossRef](#)] [[PubMed](#)]
104. Zhou, J.; Zha, X.H.; Chen, F.Y. A two-dimensional zirconium carbide by selective etching of Al₃C₃ from nanolaminated Zr₃Al₃C₅. *Angew. Chem. Int. Ed.* **2016**, *128*, 5092–5097. [[CrossRef](#)]
105. Zhao, M.Q.; Xie, X.; Ren, C.E.; Makaryan, T.; Anasori, B.; Wang, G.; Gogotsi, Y. Hollow MXene Spheres and 3D Macroporous MXene Frameworks for Na-Ion Storage. *Adv. Mater.* **2017**, *29*, 1702410. [[CrossRef](#)] [[PubMed](#)]
106. Wu, X.H.; Wang, Z.Y.; Yu, M.Z.; Xiu, L.Y.; Qiu, J.S. Stabilizing the MXenes by Carbon Nanoplatting for Developing Hierarchical Nanohybrids with Efficient Lithium Storage and Hydrogen Evolution Capability. *Adv. Mater.* **2017**, *29*, 1607017. [[CrossRef](#)] [[PubMed](#)]
107. Ghidui, M.; Lukatskaya, M.R.; Zhao, M.Q. Conductive two-dimensional titanium carbide ‘clay’ with high volumetric capacitance. *Nature* **2014**, *516*, 78–81. [[CrossRef](#)] [[PubMed](#)]
108. Ma, T.Y.; Ran, J.; Dai, S.; Jaroniec, M.; Qiao, S.Z. Phosphorus-Doped Graphitic Carbon Nitrides Grown In Situ on Carbon-Fiber Paper: Flexible and Reversible Oxygen Electrodes. *Angew. Chem. Int. Ed.* **2015**, *54*, 4646–4650. [[CrossRef](#)]
109. Ma, T.Y.; Cao, J.L.; Jaroniec, M.; Qiao, S.Z. Interacting Carbon Nitride and Titanium Carbide Nanosheets for High-Performance Oxygen Evolution. *Angew. Chem. Int. Ed.* **2016**, *55*, 1138–1142. [[CrossRef](#)]
110. Zhu, Q.L.; Xu, Q. Metal-Organic Framework Composites. *Chem. Soc. Rev.* **2014**, *43*, 5468–5512. [[CrossRef](#)]
111. Zhao, S.L.; Wang, Y.; Dong, J.C.; He, C.T.; Yin, H.J.; An, P.F.; Zhao, K.; Zhang, X.F.; Gao, C.; Zhang, L.J.; et al. Ultrathin Metal–Organic Framework Nanosheets for Electrocatalytic Oxygen Evolution. *Nat. Energy* **2016**, *1*, 16184. [[CrossRef](#)]
112. Yu, H.; Wang, Y.H.; Jing, Y. MXene-Based Nanocomposites: Surface Modified MXene-Based Nanocomposites for Electrochemical Energy Conversion and Storage. *Small* **2019**, *15*, 1970133. [[CrossRef](#)]
113. Li, Z.; Yu, L.; Milligan, C.; Ma, T.; Zhou, L.; Cui, Y.; Qi, Z.; Libretto, N.; Xu, B.; Luo, J.; et al. Two-dimensional transition metal carbides as supports for tuning the chemistry of catalytic nanoparticles. *Nat. Commun.* **2018**, *9*, 5258. [[CrossRef](#)] [[PubMed](#)]
114. Seh, Z.W.; Fredrickson, K.D.; Anasori, B.; Kibsgaard, J.; Strickler, A.L.; Lukatskaya, M.R.; Gogotsi, Y.; Jaramillo, T.F.; Vojvodic, A. Two-dimensional molybdenum carbide (MXene) as an efficient electrocatalyst for hydrogen evolution. *ACS Energy Lett.* **2016**, *1*, 589–594. [[CrossRef](#)]
115. Geng, D.C.; Zhao, X.X.; Chen, Z.X.; Sun, W.W.; Fu, W.; Chen, J.Y.; Liu, W.; Zhou, W.; Loh, K.P. Direct Synthesis of Large-Area 2D Mo₂C on In Situ Grown Graphene. *Adv. Mater.* **2017**, *29*, 1700072. [[CrossRef](#)]
116. Chaitoglou, S.; Giannakopoulou, T.; Speliotis, T.; Vavouliotis, A.; Trapalis, C.; Dimoulas, A. Mo₂C/graphene heterostructures: Low temperature chemical vapor deposition on liquid bimetallic Sn-Cu and hydrogen evolution reaction electrocatalytic properties. *Nanotechnology* **2018**, *30*, 125401. [[CrossRef](#)]
117. Yang, Y.; Wang, Y.; Xiong, Y. In Situ X-ray Absorption Spectroscopy of a Synergistic Co-Mn Oxide Catalyst for the Oxygen Reduction Reaction. *J. Am. Chem. Soc.* **2019**, *146*, 1463–1466. [[CrossRef](#)]
118. Massel, F.; Ahmadi, S.; Hahlin, M.; Liu, Y.S.; Guo, J.H.; Edvinsson, T.; Rensmo, H.; Duda, L.C. Transition metal doping effects in Co-phosphate catalysts for water splitting studied with XAS. *J. Electron Spectrosc. Relat. Phenom.* **2018**, *224*, 3–7. [[CrossRef](#)]

